

**Best  
Available  
Copy**

10

**AD-A275 227**



The Pennsylvania State University  
**APPLIED RESEARCH LABORATORY**  
P.O. Box 30  
State College, PA 16804

**A REVIEW OF SIGNAL DETECTION USING THE  
BISPECTRUM WITH APPLICATIONS IN  
UNDERWATER ACOUSTICS**

by

**G. L. Morella**

Technical Report No. TR 94-03  
January 1994

**DTIC  
ELECTE  
FEB 02 1994  
S E D**

Supported by:  
Space and Naval Warfare Systems Command

L.R. Hettche, Director  
Applied Research Laboratory

Approved for public release; distribution unlimited

**94-03360**



**94 2 01 17 6**

# REPORT DOCUMENTATION PAGE

Form Approved  
OMB No. 0704-0188

Public reporting burden for this collection of information is estimated to average 1 hour per response, including the time for reviewing instructions, searching existing data sources, gathering and maintaining the data needed, and completing and reviewing the collection of information. Send comments regarding this burden estimate or any other aspect of this collection of information, including suggestions for reducing this burden, to Washington Headquarters Service, Directorate for Information Operations and Reports, 1215 Jefferson Davis Highway, Suite 1204, Arlington, VA 22202-4302, and to the Office of Management and Budget, Paperwork Reduction Project (0704-0188), Washington, DC 20503.

|   |   |  |   |  |
|---|---|--|---|--|
| <b>1. AGENCY USE ONLY (Leave blank)</b>   |   | <b>2. REPORT DATE</b><br>January 1994                          | <b>3. REPORT TYPE AND DATES COVERED</b>                         |  |
| <b>4. TITLE AND SUBTITLE</b><br>A Review of Signal Detection Using the Bispectrum with Applications in Underwater Acoustics   |   |  | <b>5. FUNDING NUMBERS</b><br>N00039-92-C-0100                   |  |
| <b>6. AUTHOR(S)</b><br>G. L. Morella  |   |  |   |  |
| <b>7. PERFORMING ORGANIZATION NAME(S) AND ADDRESS(ES)</b><br>Applied Research Laboratory<br>The Pennsylvania State University<br>P.O. Box 30<br>State College, PA 16804   |   |  | <b>8. PERFORMING ORGANIZATION REPORT NUMBER</b><br><br>TR#94-03 |  |
| <b>9. SPONSORING / MONITORING AGENCY NAME(S) AND ADDRESS(ES)</b><br>Space and Naval Warfare Systems Command<br>Department of the Navy<br>Washington, DC 20363-5100  |   |  | <b>10. SPONSORING / MONITORING AGENCY REPORT NUMBER</b>         |  |
| <b>11. SUPPLEMENTARY NOTES</b>  |   |  |   |  |
| <b>12a. DISTRIBUTION / AVAILABILITY STATEMENT</b><br><br>Unlimited  |   |  | <b>12b. DISTRIBUTION CODE</b>                                   |  |
| <b>13. ABSTRACT (Maximum 200 words)</b><br><br>This paper reviews attempts at signal detection in Gaussian noise using a higher order statistical (Higher Order Spectra (HOS) or polyspectra) technique. Examples comparing power spectral and bispectral analysis include the following topics: the identification of signals generated by a system of coupled nonlinear differential equations, radar backscatter processing and target identification, and a statistical treatment of the detection of narrowband harmonic components resulting in a Receiver Operating Characteristic (ROC) curve.<br><br>The critical signal and noise probability density function (pdf) assumptions from polyspectra theory which must be met for more effective noise suppression relative to classical second order power spectral methods are: (1) discussed in relation to detection results as reported in the literature review; and, (2) illustrated via examples using both direct and indirect nonparametric Discrete Fourier Transform (DFT) bispectrums employing Fast Fourier Transforms (FFT) for both simulated and real data. The signal set consisted of pure tones and a hop code used in active sonar. |   |  |   |  |
| <b>14. SUBJECT TERMS</b><br>signal detection, bispectrum, unerwater acoustics, gaussian noise, higher order spectra, polyspectra  |   |  | <b>15. NUMBER OF PAGES</b><br>86                                |  |
|   |   |  | <b>16. PRICE CODE</b>   |  |
| <b>17. SECURITY CLASSIFICATION OF REPORT</b><br>UNCLASSIFIED  | <b>18. SECURITY CLASSIFICATION OF THIS PAGE</b><br>UNCLASSIFIED | <b>19. SECURITY CLASSIFICATION OF ABSTRACT</b><br>UNCLASSIFIED | <b>20. LIMITATION OF ABSTRACT</b><br>UNLIMITED                  |  |

**ABSTRACT**

This paper reviews attempts at signal detection in Gaussian noise using a higher order statistical (Higher Order Spectra (HOS) or polyspectra) technique. Examples comparing power spectral and bispectral analysis include the following topics: the identification of signals generated by a system of coupled nonlinear differential equations, radar backscatter processing and target identification, and a statistical treatment of the detection of narrowband harmonic components resulting in a Receiver Operating Characteristic (ROC) curve.

The critical signal and noise probability density function (pdf) assumptions from polyspectra theory which must be met for more effective noise suppression relative to classical second order power spectral methods are: (1) discussed in relation to detection results as reported in the literature review; and, (2) illustrated via examples using both direct and indirect nonparametric Discrete Fourier Transform (DFT) bispectrums employing Fast Fourier Transforms (FFT) for both simulated and real data. The signal set consisted of pure tones and a hop code used in active sonar.

The results are in agreement with the examples reviewed which concluded that no processing gain is derived from bispectral analysis. It is shown that the resolution for direct methods using no formal cumulant construction (for zero mean strictly stationary random processes, cumulants up to third order are equal to moments up to third order) was far superior to that of indirect methods containing third order cumulant sequences. Simulated and real tests indicate no significant improvement in bispectral over power spectral analysis because the echoed signals exhibited a symmetric pdf (skewness approximately zero) similar to Gaussian noise. In theory the bispectrum cannot differentiate between non-Gaussian symmetric signals and Gaussian or non-Gaussian symmetric noise, all of which are equally suppressed. Noise only suppression

occurs when the signals echoed or radiated are zero-mean non-Gaussian with non-zero skewness (no symmetry evident), and the noise is zero-mean Gaussian or non-Gaussian with zero skewness (symmetry evident).

The efficacy of signal detection in underwater acoustics using polyspectral methods is examined in the light of current research into nonstationary HOS with future directions for study indicated.

|                    |                                     |
|--------------------|-------------------------------------|
| Accession For      |                                     |
| NTIS CRA&I         | <input checked="" type="checkbox"/> |
| DTIC TAB           | <input type="checkbox"/>            |
| Unannounced        | <input type="checkbox"/>            |
| Justification      |                                     |
| By                 |                                     |
| Distribution /     |                                     |
| Availability Codes |                                     |
| Dist               | Avail and/or Special                |
| A-1                |                                     |

DTIC QUALITY INSURANCE

## TABLE OF CONTENTS

|                               |   |      |
|-------------------------------|---|------|
| <b>Abstract</b> .....         |   | iii  |
| <b>Acknowledgements</b> ..... |   | viii |
| <b>Chapter 1.</b>             | <b>INTRODUCTION</b> .....   | 1    |
| <b>Chapter 2.</b>             | <b>A REVIEW OF DETECTION RESULTS AS REPORTED<br/>IN LITERATURE</b> .....  | 8    |
|                               | 2.0.1 Identification of Signals Generated by a Coupled System of<br>Nonlinear Differential Equations .....  | 8    |
|                               | 2.0.2 Radar Backscatter Processing and Target Identification .....  | 10   |
|                               | 2.0.3 Statistical Treatment of the Detection of Narrowband<br>Harmonic Components Resulting in a Receiver<br>Operating Characteristic (ROC) Curve ..... | 15   |
|                               | 2.1 Nonparametric Methods .....   | 19   |
|                               | 2.1.1 Direct Method .....   | 20   |
|                               | 2.1.1.1 Test Results .....  | 25   |
|                               | 2.1.2 Indirect Method .....   | 26   |
|                               | 2.1.2.1 Test Results .....  | 29   |
|                               | 2.2 Parametric Methods .....  | 30   |
|                               | 2.2.1 Harmonic Retrieval Test Results .....   | 31   |
| <b>Chapter 3.</b>             | <b>CONCLUSIONS/FUTURE WORK</b> .....  | 33   |
|                               | 3.0 General Conclusion .....  | 33   |
|                               | 3.1 Nonstationary Higher-Order Spectra .....  | 34   |
|                               | 3.1.1 Conclusion .....  | 35   |
|                               | 3.1.2 Future Work .....   | 36   |
|                               | 3.2 Trispectrum .....   | 36   |
|                               | 3.2.1 Conclusion .....  | 40   |
|                               | 3.2.2 Future Work .....   | 40   |

**TABLE OF CONTENTS (Continued)**

|   |           |
|---|-----------|
| <b>REFERENCES</b> .....   | <b>46</b> |
| <b>Appendix A. HI-SPEC</b> .....  | <b>53</b> |
| <b>A.0 Software Description</b> .....                                     | <b>54</b> |
| <b>A.1 Bispectrum Routines</b> .....                                      | <b>56</b> |
| <b>A.2 Gaussianity Tests</b> .....  | <b>57</b> |
| <b>A.3 Harmonic Estimation</b> .....                                      | <b>58</b> |
| <b>Appendix B. POLYSPECTRA THEORY</b> .....                               | <b>60</b> |
| <b>B.0 Introduction</b> .....   | <b>61</b> |
| <b>B.1 Moments and Cumulants</b> .....                                    | <b>61</b> |
| <b>B.2 Higher-Order Spectra</b> .....                                     | <b>64</b> |
| <b>Appendix C. SIMULATED/REAL DATA TEST RESULTS</b> .....                 | <b>75</b> |
| <b>C.0 Power Spectrum/Bispectrum Comparison for Simulated Data</b> .....  | <b>76</b> |
| <b>C.1 Direct/Indirect Bispectrum Comparison for Simulated Data</b> ..... | <b>76</b> |
| <b>C.2 Power Spectrum/Bispectrum Comparison for Real Data</b> .....       | <b>78</b> |

## LIST OF FIGURES

|                        |   |    |
|------------------------|---|----|
| <b>Figure 2.0-1.</b>   | <b>Comparison of Bispectrum and Power Spectrum<br/>Detection Performance for PFA = 0.001</b>                                    | 19 |
| <b>Figure 2.1.1-1.</b> | <b>Rao-Gabr Window Bounds</b>   | 25 |
| <b>Figure B.2-1a.</b>  | <b>The Six Symmetry Regions of the Third Order<br/>Cumulant Function</b>  | 70 |
| <b>Figure B.2-1b.</b>  | <b>The Twelve Symmetry Regions of the Bispectrum</b>  | 70 |
| <b>Figure B.2-2.</b>   | <b>Fundamental Domain of Discrete Time Bispectrum</b>   | 71 |
| <b>Figure B.2-3.</b>   | <b>Distribution of the Responses in the Bispectral<br/>Domain as a Function of Third Order Cumulant<br/>Conjugate Placement</b> | 72 |
| <b>Figure C.0-1.</b>   | <b>Power Spectrum/Bispectrum Comparison for<br/>Simulated Data - Noiseless</b>  | 80 |
| <b>Figure C.0-2</b>    | <b>Power Spectrum/Bispectrum Comparison for<br/>Simulated Data - Low Noise</b>  | 81 |
| <b>Figure C.0-3</b>    | <b>Power Spectrum/Bispectrum Comparison for<br/>Simulated Data - High Noise</b>   | 82 |
| <b>Figure C.1-1</b>    | <b>Direct/Indirect Bispectrum Comparison for<br/>Simulated Data - Noiseless</b>   | 83 |
| <b>Figure C.1-2</b>    | <b>Direct/Indirect Bispectrum Comparison for<br/>Simulated Data - Noise</b>   | 84 |
| <b>Figure C.2-1</b>    | <b>Power Spectrum/Bispectrum Comparison for<br/>Real Data - Hop Code</b>  | 85 |
| <b>Figure C.2-2</b>    | <b>Power Spectrum/Bispectrum Comparison for<br/>Real Data - Pure Tone</b>   | 86 |

## CHAPTER 1

### INTRODUCTION

Power spectral information is that which is present in the second-order statistics or autocorrelation domain which suffices for the complete statistical description of a Gaussian process of known mean. Phase information is suppressed in the autocorrelation domain since the signal in question is represented as a superposition of statistically uncorrelated harmonic components. Situations may exist, however, when the minimum-phase assumptions of second-order statistics do not suffice, i.e., non-minimum phase information needs to be extracted as well as deviations from Gaussianity and degrees of nonlinearities. For these cases, higher-order spectra such as the bispectrum and trispectrum are required.

Higher order spectra or polyspectra are the  $(n-1)$  dimensional Fourier transforms of  $n$ th order cumulant sequences.<sup>16</sup> Cumulants are phase sensitive higher order statistics which are useful in the analysis and description of non-Gaussian processes. They display the degree of higher order correlation present in a random series as well as providing a measure of the deviation of a particular distribution from Gaussianity.

In general, the three main motivations behind the use of polyspectra in signal processing are: (1) Gaussian noise suppression for processes of unknown spectrum characteristics in detection, parameter estimation, and classification problems; (2) phase and magnitude response reconstruction of signals; and (3) detection and characterization of time series nonlinearities. The first motivation will be the focus of this paper and is based on the property that for Gaussian processes only, all higher-order spectra of order greater than two are identically zero.<sup>15</sup> This leads to the conjecture that for applications where the observed waveform consists of a non-Gaussian signal with non-zero skewness in additive Gaussian noise

or a non-Gaussian signal with non-zero skewness in non-Gaussian noise with zero skewness, certain advantages may exist in signal detection in polyspectra domains.<sup>2</sup>

Higher-order spectra (polyspectra) defined in terms of the higher-order moments or cumulants of a signal (see Appendix B for definition of cumulants and joint cumulants) can be used to examine more information contained in a stochastic non-Gaussian or deterministic signal than is contained in its autocorrelation (power spectrum). From statistical theory we know that all joint cumulants higher than the second order vanish for a multivariate normal process.<sup>15</sup> The immediate impact of this is that all spectra of order higher than two vanish for a Gaussian process. Thus, higher-order spectra appear useful in distinguishing non-Gaussian processes embedded in Gaussian noise. Moreover, polyspectra retain phase and give a measure of the phase correlation between components whose frequencies sum to zero. Such phase relations could occur due to nonlinearities arising from modulation effects of active sonar signals or from the output of a quadratic system that contains power contributions at frequencies which are sums or differences of pairs of input frequencies, a phenomenon known as Quadratic Phase Coupling (QPC).<sup>15</sup> QPC could result from the interaction of ship systems giving rise to tonals (harmonics) above broadband noise in the passive sonar case. As an example of this consider the frequency triple ( $f_1, f_2, f_3=f_1+f_2$ ). Quadratic coupling would result in a power contribution at  $f_3$  if the phase at  $f_3$  was the sum of the phases at  $f_1$  and  $f_2$ . The bispectrum identifies quadratic nonlinearities of this type while the power spectrum is completely insensitive to such phase relations.

There are basically two ways that can be used to estimate higher-order spectra when a finite set of observation measurements is available, conventional (Fourier or nonparametric) methods and the parametric approach based on Autoregressive (AR), Moving Average (MA), and Autoregressive Moving Average (ARMA) models. Conventional approaches can be

implemented either by direct or indirect methods. The direct method refers to direct generation of the DFT coefficients required for the ensemble average of the bispectral triple product from the input data. It does not require using the 2-D FFT. The indirect method refers to the generation of cumulants from the input data which are subsequently double Fourier transformed to give the bispectrum. It comes from the general definition of polyspectra being  $(n-1)$  dimensional Fourier transforms of  $n$ th order cumulant functions. In the case of bispectra, this reduces to a 2-D Fourier transform of a third order cumulant function. (See sections 2.1.1 and 2.1.2). The direct method as a natural starting point for polyspectra analysis is the main focus of this paper with the conventional indirect method and parametric techniques briefly examined for comparison purposes.

Few applications of polyspectra have arisen due to the voluminous nature of the data requirements with the accompanying computational burden. Also, statistical difficulties coupled with the lack of a physical understandable interpretation have compounded the problem.

For our purposes we will only be concerned with the fact that if a time series has a statistically significant bispectrum, the generating process is non-Gaussian with a sufficient degree of skewness as to be prominent in a Gaussian or non-Gaussian symmetric probability density function (pdf) background which will result in a vanishing bicoherence. (See Appendix A). Bicoherence analysis results when the bispectrum shows a sensitivity to the amplitudes of the involved spectral components.<sup>5</sup> It has been shown that, for even incoherent signals, the value of the bispectrum can be significant if averaging is performed on too small a number of records. Since the bispectral estimator can be misleading, normalized bispectrums or bicoherences are the preferred choice of analysts as a function of processing capabilities. Bicoherence, however, is very sensitive to SNR because of the normalization. This is

observed when, for perfectly coherent signals, the bicoherence is not one due to the input noise. If the SNR is low, the value of the bicoherence estimated with a relatively small number of data records, e.g.,  $K < 50$ , can be insignificant. To recover significant value the number of data records must be increased (up to several hundred) at least if the signal is stationary over a sufficiently long time interval.<sup>5</sup> This can prove prohibitive which is the reason why bispectral sensitivity to amplitudes of spectral components is tolerated. Moreover, what is an undesirable feature for some is advantageous for others as this same amplitude sensitivity is the main reason that uncoupled harmonics are prominent above noise in the bispectrum. The real problem is why aren't such signals more prominent given the "vanishing" nature of bispectrums and/or bicoherences to Gaussian processes. The literature would seem to imply that a processing gain is inherent in the application of polyspectral methods. The answer is that theory is seldom realized in practice for the reasons cited by Lagoutte in Reference 5 and reported here. It is interesting to note Lagoutte's conclusion, "it can be said that the use of bispectrum analysis can be subject to wrong interpretation. Bicoherence can only be used if the waves are not embedded in noise." This author has not seen too many physical processes over the course of his career that are not embedded in significant noise of some type other than those idealized results which invariably turn up in journal articles but, strangely enough, are never applied to actual physical systems.

Our main interest in the use of polyspectra is the realization of an improvement relative to second order methods in the suppression of additive Gaussian noise for signal detection problems arising in underwater acoustics.<sup>22</sup> Non-Gaussian signal processes occur for active sonar when the reflecting target has only a few dominating scatterers. The noise in such applications is frequently Gaussian, so that the detection problem is that of detecting a non-Gaussian signal embedded in additive Gaussian noise.

Detection problems related to non-Gaussian noise<sup>22</sup> include sonars operating under ice where noise due to ice-cracking, creaking and floe-smashing contribute a component found to have substantial non-Gaussian behavior. Additionally, active sonars operating under ice near the surface may encounter a non-Gaussian component due to specular reflection from the irregular under-ice surface. Another environmental situation which may produce non-Gaussian noise is shallow-water reverberation. Theoretically, non-Gaussian noise can be equally suppressed via conventional polyspectral methods if the noise possesses a symmetric pdf, i.e., is not highly skewed.<sup>2</sup>

This paper will address problems related to active sonar as defined in reference 22 when the noise background is reverberation-limited and the scatterers giving rise to the reverberation are assumed to be statistically independent in their reflecting properties. Application of the central limit theorem gives rise to a Gaussian process for reverberation while the return, being primarily due to reflections from a few random scatterers will be compositely non-Gaussian.

In passive sonar<sup>22</sup> the detection of non-Gaussian signals in Gaussian noise occurs when the background noise is frequently assumed to be Gaussian and stationary with the sources such as ship-radiated noise being non-Gaussian. The passive problem is not considered in this paper.

Hi-Spec, a collection of Matlab M-files designed to be used in conjunction with Matlab developed by the MathWorks,<sup>12,13</sup> is a software package which provides polyspectra analysis capabilities for various processing applications.<sup>1,2</sup> A brief description of Hi-Spec routines is given in Appendix A. The routines specifically used for this paper included "bispec\_d" - direct method for bispectrum estimation, "bispec\_i" - indirect method for bispectrum estimation, "gl\_stat" - detection statistics for Hinich's Gaussianity and linearity

tests, "qpc\_gen" - generator for quadratically phase-coupled harmonics in noise, "harm-gen" - generator for harmonics in Gaussian (colored) noise for the harmonic retrieval problem, and "harm\_est" - estimator of power spectra harmonics using MUSIC, Eigenvector, Pisarenko, ML (Capon) and AR methods based on the diagonal slice of the fourth order cumulant with conventional periodogram also give for comparison purposes.

The routine "qpc\_gen" generated the data for Figures C.1-1 and C.1-2 in Appendix C as described in section C.1 **DIRECT/INDIRECT COMPARISON FOR SIMULATED DATA.**

The routine "bispec\_d" was used to calculate the direct bispectrum for: (1) Figures C.0-1, C.0-2, and C.0-3 in Appendix C as described in section C.0 **POWER SPECTRUM/BISPECTRUM COMPARISON FOR SIMULATED DATA,** (2) Figures C.1-1 and C.1-2 in Appendix C as described in section C.1 **DIRECT/INDIRECT BISPECTRUM COMPARISON FOR SIMULATED DATA,** and (3) Figures C.2-1 and C.2-2 in Appendix C as described in section C.2 **POWER SPECTRUM/BISPECTRUM COMPARISON FOR REAL DATA.**

The routine "bispec\_i" was used to calculate the indirect bispectrum for Figures C.1-1 and C.1-2 in Appendix C as described in section C.1 **DIRECT/INDIRECT COMPARISON FOR SIMULATED DATA.**

The routine "gl\_stat" was used as an added, albeit redundant check due to the observed obvious non-zero nature of the echoed signal skewness, to verify the zero skewness hypothesis for the real data as described in section C.2 **POWER SPECTRUM/BISPECTRUM COMPARISON FOR REAL DATA.** The use of the "gl\_stat" routine in this context was more for security than an absolute requirement and, as such, not formally addressed in this paper. It will suffice to say that "gl\_stat" verified the zero skewness hypothesis in all

instances which gave the author a warm feeling about the "correctness" of the Hi-Spec software package. It is worth noting that there are many statistical tests of a less complicated nature than "gl\_stat" which serve the same purpose, i.e., the comparison of continuous or binned data where one data set is compared to a known distribution or two equally unknown data sets are to be compared. See Chi-Square goodness-of-fit and Kolmogorov-Smirnov tests as described in reference 52.

The routine "harm\_gen" was used to generate the harmonics for the higher order statistical resolution improvement routine "harm\_est" as reported in section 2.2.1 Harmonic Retrieval. The results were briefly addressed for illustrative purposes to make the reader aware that higher order statistical versions of these routines suffer from the same constraints that their lower order counterparts do - namely a high SNR requirement. This coupled with a lack of signal skewness caused no discernable difference with second order periodogram methods.

A condensed version of this paper was published in *The U. S. Navy Journal of Underwater Acoustics*, Volume 43, No. 1, January 1993, pp. 201-220, under the title, "Signal Detection Using the Bispectrum."

## CHAPTER 2

### A REVIEW OF DETECTION RESULTS AS REPORTED IN LITERATURE

This chapter reviews nonparametric and parametric attempts at signal detection in Gaussian noise using the bispectrum. Examples from the literature which address comparison of power spectral to bispectral methods include the following applications: (1) the identification of signals generated by a system of coupled nonlinear differential equations, (2) radar backscatter processing and target identification, and (3) a statistical treatment of the detection of narrowband harmonic components resulting in a Receiver Operating Characteristic (ROC) curve. The nonparametric direct and indirect methods are formally defined along with corresponding test results which are in agreement with the examples cited in the literature review. Parametric methods are described including the reasons for neglecting same in this paper. Harmonic retrieval is briefly discussed in the context of conjectured resolution enhancements due to applying higher order statistics to standard algorithms. The resolution section is included to show the extension of the detection problem, lack of signal skewness compared to noise, to the resolution problem.

#### 2.0.1 Identification of Signals Generated by a Coupled System of Nonlinear Differential Equations

The detectability of signals was examined through experiments in which simulated signals were subjected to power-spectral and direct bispectral analysis.<sup>11</sup> Specifically, signals rich in harmonic content were generated by solving a system of coupled nonlinear differential equations and were subsequently contaminated by Gaussian white noise before being subjected to spectral and bispectral analysis. The effects of start up transients due to initial conditions

were removed by discarding the first 2,000 points as the solution was stepped for typically 10,000 steps. Classical windowing and segment averaging was applied to the noise cases for two different noise levels described as low and high. In both instances ensemble averaging did not produce sufficient reduction of background noise to make the bispectrum a significantly more efficient signal detector than the power spectrum. It was concluded that the bispectrum slices taken did not show it to be a very valuable indicator of the existence of multiple harmonic signals in the presence of Gaussian noise. No signals were observed in the presence of noise using bispectra when they were not also visible in the power spectra. It was further shown that no increase in processing gain is derived from bispectral analysis even though it makes use of inter-frequency phase relation data. It was found that reliable detection required more signal energy in the bispectral case than for spectral detection unless the signal skewness was large. The amount of averaging applied to reduce random sampling variations is proportional to the time bandwidth product. The disadvantage of bispectral analysis varied directly with the time bandwidth product as results indicated that the bispectral detector was inferior to both energy and correlation (matched filter) detectors. Bispectra did not appear to offer any advantage in detectability at low signal-to-noise ratios unless the signal skewness was large.

As a caveat it was pointed out<sup>11</sup> that the signal bispectrum contained more structure than the power spectrum, indicating that bispectral analysis of signals may provide useful additional classification beyond that obtained from energy methods. It was further conjectured that bispectral analysis may be useful in active acoustic detectors in the presence of reverberation assuming that the acoustic return reflects a localization compared with the reflectors producing reverberation.

## **2.0.2 Radar Backscatter Processing and Target Identification**

The use of bispectral processing methods for radar backscatter processing and target identification have also been examined.<sup>23</sup> In this situation bispectral processing methods were adapted to the radar signature analysis problem which resulted in the birange profile, a 2-D display of target scattering mechanisms in the range domain with the final goal being the detection and classification of radar signals.

The type of signal processing addressed in this study is based on a specific target scattering model where the scattered signal is a combination of specular scattering terms from localized areas on the target and multiple interaction terms. Higher order spectral processing of radar signatures, similar to classical spectral analysis of radar data, produces signatures in the time domain that are related to the geometrical shape of the target. This serves as an aid in target discrimination. A description of this process follows.

Complex natural resonances of radar targets are aspect independent and are used as an aspect insensitive method for discriminating between targets. No information about the scattering mechanisms of a radar target is directly evident from the backscattered frequency response data. However, this information pertaining to target shape, size and orientation is present in frequency and can be extracted by examining the target scattering mechanisms that are displayed in the Target Impulse Response (TIR). The TIR comes into play since if a plane wave is transmitted to illuminate a target, then the backscattered field is a function of the transfer function as seen by the radar, and the range to the target. Accordingly, it is desirable to change variables from frequency to time since target scattering features can be recovered from the impulse response giving the analyst a more intuitive understanding of the processes involved by working with time domain signatures instead of frequency domain responses. For the radar problem the end result becomes a time triple correlation mapped to a range plane via

the bispectrum where the bispectrum is expressed as an ensemble average of impulse responses  $B(r_1, r_2) = \langle h(r_1)h(r_2)h(r_1+r_2) \rangle$  where  $h(r)$  is the impulse response as a function of range. Defining the birange as such implies that a non-zero bispectral response is the result of interaction between the responses at ranges  $r_1$  and  $r_2$  which appear as a response at the range  $r_1+r_2$ . For the bispectrum of real data, this usually takes the form of a clearly evident non-zero magnitude bispectrum at the ordered pair in range  $(r_1, r_2)$  in the principal triangular region of the bispectrum (see appendix B), and various assorted other ordered pairs in the corresponding eleven bispectrum symmetry regions. (See Figure B.2-1b.) These symmetry regions containing significant non-zero magnitude bispectrums occur at the ordered pairs:  $(r_2, r_1)$  from symmetry region 2,  $(-r_2, r_1+r_2)$  from conjugate symmetry region 3,  $(-r_1, r_1+r_2)$  from conjugate symmetry region 4,  $(-r_1-r_2, r_1)$  from symmetry region 5,  $(-r_1-r_2, r_2)$  from symmetry region 6,  $(r_1, -r_2)$  from conjugate symmetry region 7,  $(-r_2, -r_1)$  from conjugate symmetry region 8,  $(r_2, -r_1-r_2)$  from symmetry region 9,  $(r_1, -r_1-r_2)$  from symmetry region 10,  $(r_1+r_2, -r_1)$  from conjugate symmetry region 11, and finally,  $(r_1+r_2, -r_2)$  from conjugate symmetry region 12. (See Appendix C section C.1 figures for an illustration of the twelve symmetry regions of the bispectrum for real data.) Furthermore, the bispectrum at  $(r_1, r_2)$  is non-zero only if the responses at  $r_1$  and  $r_2$  and  $r_1+r_2$  are correlated. For the bispectrum of complex data, the non-zero magnitude of the bispectral response corresponding to the interactions between the responses at ranges  $r_1$  and  $r_2$  still appears at the ordered pair in range  $(r_1, r_2)$  located in the principal triangular region of the bispectrum as before for the real data case. However, because we are now dealing with bispectrums of complex as opposed to real data, there are no longer twelve symmetry regions but only one defined by the placement of the complex conjugate for the third order joint cumulant.<sup>23,59</sup> An example of the placement used in Hi-spec is given in Appendix B directly below Figure B.2-3. This corresponds to the

first symmetry relation defined for the bispectrum of complex-valued signals immediately following the example. Formally, this range symmetry for the complex case would only occur at  $(r_2, r_1)$  in the area designated region 2 in Figure B.2-1b in Appendix B. The noise suppression capabilities of the bispectrum arise from the fact that uncorrelated or low correlated Gaussian noise of unknown spectra characteristics (colored or white) does not have a significant bispectrum. Consequently, the motivation for using bispectrums for detection purposes becomes clear as, in theory for an infinite number of samples, Gaussian processes vanish. In practice, however, only a finite number of data samples is available so additive Gaussian noise is not totally suppressed in the birange profile. Also, since additive noise may be only asymptotically Gaussian or non-Gaussian clutter having a non-zero third order moment (skewness), total noise suppression wouldn't occur for even an infinite number of samples. The obvious conjecture is that the bispectrum might prove a viable alternative to power spectrum techniques since it retains phase information thereby identifying any type of phase coupling which might result from the interactions of target scattering mechanisms. This information could allow for better target detection. The time/range mapping is discussed next.

In most signal processing problems, the data sequence consists of samples taken from a time dependent waveform. Then the bispectrum, as defined in Appendix B, is a function of two variables in the frequency domain. The radar scattering data sequence, however, is not a time series but recorded in the frequency domain. The triple correlation of this radar frequency domain data is a 2-D profile in the frequency domain with the applied bispectrum becoming a profile of target scattering signatures in the 2-D time domain which could be termed a "bi-time" profile of radar targets. This profile can be subsequently expressed as a 2-D profile in range using the standard range equation  $r = ct/2$  where  $r$  is the range from the radar to the target,  $t$  is the time needed for the signal to propagate to the target and back, and  $c$

is the speed of light. This is what is referred to as the birange profile of the target. Formally, it is a bispectral display of target signatures in the 2-D range domain  $r_1$  and  $r_2$  where the term "range" denotes the propagation distance to the target. This process is directly related to the classical problem of determining the system impulse response by taking the inverse Fourier transform of the system transfer function (analogous to the radar system transfer function containing the complex natural resonances of the targets). This resulting time triple correlation is subsequently mapped to range to create the birange profile.

The focus of the report was on the processing of radar data treated as a time series using higher order spectral analysis techniques, in particular, the bispectrum. The reason for the renewed interest in the bispectrum as a general signal processing technique is related to current increases in processing capabilities as, previously, excessive computational requirements gave the promise of limited rewards. Not only are the mathematics of the bispectrum far more complicated than for other spectral analysis techniques but the physical insight into the technique is not fully understood as the main problem remains the lack of an intuitive interpretation and understanding of the bispectral processing of a time series.

Both Direct and Indirect methods of bispectrum computation were outlined with the requirement for a large number of data samples due to the high variance incurred by both estimates. It was noted that the estimates could be made smoother if more data segments were used at the expense of decreased birange resolution that results from the introduction of nonstationary problems. The main advantage of these methods is the ease of implementation using FFT algorithms. A variant of these methods was used to generate the birange profiles. A parametric technique using autoregressive modeling was introduced as an alternative to classical Fourier transform techniques. The reasons for this stemmed from the resolution of the estimated profiles being limited by bandwidth and the effects of the window function used.

(The window had a wide mainlobe which further limited resolution.) It was pointed out that applying a rectangular window to the triple correlation for the bispectrum caused 2-D sidelobes to appear along each range axis. It was observed that with finite sets of radar scattering data, resolution problems with Fourier techniques are inevitable. To avoid this problem the parametric technique was imposed which assumed that the scattering as a function of frequency satisfies a model whose parameters are estimated from the measured data. The birange resolution was no longer limited by the measurement bandwidth as was the case with Fourier based processing of finite length data records. The parameters in question were autoregressive (AR) and could be estimated from the second or third order cumulants of the measured backscatter data sequence. The birange was then computed as the triple correlation of the inverse Z transform of the measured backscatter response which became the Target Impulse Response (TIR). Hence, the birange was parameterized by the AR coefficients. The limitations of parametric modeling arose from the fact that: (1) scattering at frequencies outside the measurements can not be easily predicted from the measured data due to dependence on many factors such as dispersion and scattering region, and (2) model parameters are often estimated using nonlinear algorithms and, as such, are sensitive to noise in the data. It was noted that improvements in Fourier methods could be achieved if the measured backscatter had a high signal-to-noise ratio coupled with a slowly varying frequency response for the target.

An AR parametric model where the parameters were estimated using third order cumulants was devised and tested using experimental radar data. The AR birange profiles were compared to the Fourier transform based birange estimates. The results obtained on modeling scaled model aircraft using the AR-based algorithm were not encouraging in the sense that no closely spaced peaks in the birange were resolved and little compatibility

between Fourier-based birange profiles and AR-based birange profiles was observed. This incompatibility was attributed to problems associated with modeling complex (bispectral, i.e., birange) as opposed to spectral data. For a detailed discussion on the problems associated with the AR modeling of complex-valued signals see section 4.3 of Jouny.<sup>23</sup>

The motivation for bispectral processing of radar signals for this study<sup>23</sup> was the inherent advantage over spectral processing techniques for the suppressing of additive Gaussian noise or any additive undesirable random signal with a symmetric pdf. This engendered the interest in using birange profiles for target recognition purposes, in particular, if the backscatter waveforms are corrupted with zero mean additive Gaussian noise. The process of target recognition was approached in two ways: nonparametric FFT-based and parametric AR modeled. The parametric approach required the knowledge of the underlying distribution of the birange profile and the apriori probability of occurrence of each target. Such an approach was deemed useful for estimating the optimal classification performance that could be achieved using the birange as a feature. However, due to the lack of knowledge of the apriori probabilities of possible targets, and due to the computational burden imposed by parametric classification, nonparametric classifiers are often more appropriate.

In summary, it was found that performance gains using the birange profile were slight with the additional computational needs being an undesirable tradeoff.<sup>23</sup>

### **2.0.3 Statistical Treatment of the Detection of Narrowband Harmonic**

#### **Components Resulting in a Receiver Operating Characteristic (ROC) Curve**

A comparison of the detection performance of the power spectrum and bispectrum for detecting narrowband harmonic components is given in Wilson.<sup>29</sup> The emphasis here is on a more statistical treatment of the detection process. Consistent estimates of the unnormalized

bispectrum are constructed as a function of the number of DFTs over which the bispectrum is coherently averaged. Normalized bispectrums, i.e. bicoherences [see (A.2-1) and B.2-10)], are also considered. The variance of the unnormalized bispectral estimator becomes a function of the multiple of the power spectrums at the respective bispectral frequencies  $f(j)$ ,  $f(k)$ , and  $f(j+k)$  scaled by the DFT size divided by the number of DFTs averaged. The time series is assumed to be uncorrelated in time. The coherently averaged estimator of the bispectrum is shown to be an element of a multivariate complex Wishart distribution with dimension 3, degrees of freedom corresponding to the number of averaged bispectrums, and complex Gaussian distributed in the asymptotic sense. The bicoherence is determined to produce a quantity whose asymptotic statistics are more easily calculated. It is pointed out that since the asymptotic distribution of the bispectral estimator is complex Gaussian, the distribution of the bicoherence is given by an asymptotically noncentral chi-square distribution with two degrees of freedom and a noncentrality parameter which is a function of the skewness of the data in the time series in question, e.g. if the time series is Gaussian, the skewness function will be zero for all bispectral frequency pairs and the distribution of the bicoherence (normalized bispectrum) is central chi-square with two degrees of freedom (the noncentrality parameter will also be zero). For the detection of signals in the presence of additive Gaussian noise, a threshold is applied to the bicoherence estimate to detect a non-zero bispectrum at a specified false alarm rate corresponding to the probability of committing a Type I error (accepting the alternative hypothesis when the null is true) from the central chi-square distribution. The derivation of the noncentrality parameter as a function of the skewness of the signal and the signal-to-noise power ratio for a noncentral chi-square distributed normalized bispectrum estimate of signal-plus-noise is given in Hinich.<sup>31</sup> The probability of detection is then computed for the normalized bispectrum (bicoherence) from the noncentral chi-square

distribution as a function of the noncentrality and the threshold parameters for the noncentral chi-square distribution. A similar threshold is derived as a function of the signal-to-noise power ratios at the  $f(j)$ ,  $f(k)$ , and  $f(j+k)$  bispectral frequencies for the magnitude squared unnormalized bispectrum to calculate the probability of detection from the noncentral chi-square distribution by evaluating the probability that a noncentral chi-square random variable with a given non-centrality parameter will exceed the normalized bispectrum threshold which is, in turn, normalized by the aforementioned bispectral frequency signal-to-power ratios. Simply put, the concern is how large the normalized bispectrum statistic has to be in order to confidently reject the "Gaussian noise only" hypothesis in favor of declaring the presence of a non-Gaussian signal. It is shown<sup>29</sup> that to operate at a false alarm rate of .001, one would reject the hypothesis that only noise is present (the normalized bispectrum statistic is central chi-square distributed rather than noncentral chi-square distributed) for values of the normalized bispectrum statistic that are 13.8 or larger. The observation is made that since the mean value of the normalized bispectrum statistic is equal to the noncentrality parameter, it follows that the noncentrality parameter must be 13.8 or larger to achieve detection at this false alarm rate. The critical issues addressed<sup>29</sup> from a statistical perspective pertain to this noncentrality parameter, in particular, the several factors which contribute to its value-- skewness (characteristic of the signal), signal-to-noise ratio (characteristic of the signal and noise power levels), and finally, the processing characteristics, i.e., DFT size, number of DFTs used in bispectrum averaging.

The conclusions reached<sup>29</sup> can be summarized as follows. If a signal has a non-zero skewness function, a tradeoff exists between signal-to-noise ratio and processing parameters which will determine if the non-zero skewness is sufficiently large to result in a noncentrality parameter which will allow its detection at a given false alarm rate. For small values of the

skewness function, the processing parameters and signal-to-noise ratios have to be such that their product remains large enough to produce a sufficiently large noncentrality parameter for detection. [The noncentrality parameter has a linear dependence on the number of averages and an approximately cubic dependence on signal-to-noise ratio (for low SNR).] The implication here is that if the signal-to-noise ratio decreases by a factor of 2 (3 dB), then it is necessary to increase the number of averages by a factor of 8 in order to retain the same level of detectability dictating a certain degree of flexibility for real time algorithmic realizations which may not be feasible. By far, it is clear that the underlying concern remains signal skewness as Wilson<sup>29</sup> demonstrates the essential relationship between signal characteristics, noise characteristics, and processing parameters which define the detection performance of the bispectrum. It is shown that given a skewness function, the processing parameters necessary to achieve detection as a function of signal-to-noise ratio can be determined. Broadband detection in which the detection statistic is based on bispectrum values over the entire principal domain is discussed in Hinich<sup>31</sup> as opposed to narrowband detection at a single point in the bispectrum.

A comparison of the detection performance of both the normalized and unnormalized bispectrum to the power spectrum for detecting harmonics in Gaussian noise is shown in the Figure 2.0-1 from Wilson.<sup>29</sup> This figure is based on three harmonics having the same signal-to-noise ratio. The number of averages used was 10 necessitating an approximation to the asymptotic statistics used to produce the results since the expression for the exact distribution has not been derived. The unnormalized bispectrum (B) performs better than the power spectrum (PS) while the normalized bispectrum (NB) performs worse. The best that can be said about bispectral estimation based upon this ROC (Receiver Operating Characteristic) curve is that it is no better than approximately 2-2.5 dB over power spectral techniques in the

signal-to-noise ratio range of -10 to 10 dB with a normalized version up to 8 dB worse on the high end. It is worth noting that Wilson assumed that all of the variables critical to successful bispectral processing are optimal, i.e., sufficient signal skewness exists, the noise is Gaussian or non-Gaussian symmetric, and the processing parameters (DFT length, number of DFTs averaged, etc.), are chosen such that detection will result from a sufficiently large noncentrality parameter for the noncentral chi-square distribution in those cases where the skewness function is low.

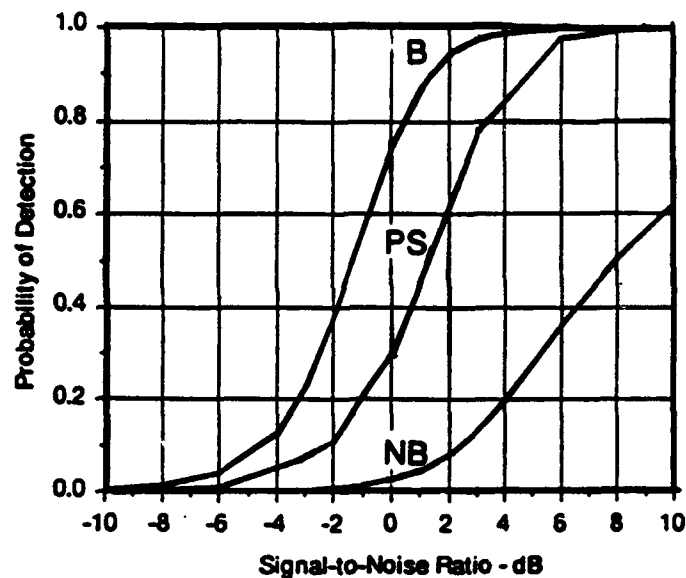


**Figure 2.0-1 Comparison of Bispectrum and Power Spectrum Narrowband Detection Performance for PFA = 0.001**

## 2.1 NONPARAMETRIC METHODS

The methods can be broken down into two classes, direct and indirect. The methods have the advantage of being straight forward allowing the introduction of polyspectral processing from a computational standpoint which is comparable to the well known classical Discrete Fourier Transform (DFT) implementation of the power spectrum.

In practice, conventional bispectrum estimators<sup>15</sup> use a finite set of observation measurements. However, the caution is that limitations on the statistical variance of the estimates, computer time and memory requirements present severe implementation problems. In general, the direct and indirect methods for bispectrum estimation give different statistical estimates. These estimates, however, are asymptotically unbiased and consistent and have distributions that tend to be complex Gaussian.<sup>16</sup> Conventional estimators have high variance and thus require a large number of records to obtain smooth bispectral estimates. Increasing the number of records or segments causes the tradeoff of increased computation time and can present additional problems with nonstationarities. Frequency domain averaging over small rectangles to reduce variance has the unwanted side effect of increasing bias as well as computation time. As per power spectrum computations, the effective number of records can be increased by overlapping for short data records.<sup>15</sup>

### 2.1.1 Direct Method

This class of conventional estimator is useful for the generation of moment spectra using FFT algorithms and is defined in Nikias<sup>16</sup> as follows.

Let  $\{X(1), X(2), \dots, X(N)\}$  be the available set of observations for bispectrum estimation. Assume that  $f_s$  is the sampling frequency and  $\Delta_o = f_s/N_o$  is the required spacing between frequency samples in the bispectrum domain along horizontal or vertical directions. Thus  $N_o$  is the total number of frequency samples.

1. Segment the data into  $K$  segments of  $M$  samples each, that is  $N = KM$ , and subtract the average value of each segment. If necessary, add zeros at each segment to obtain a convenient length  $M$  for the FFT.

2. Assuming that  $\{x^{(i)}(k), k=0,1,2,\dots,M-1\}$  are the data of segment  $\{i\}$ , generate the DFT coefficients

$$Y^{(i)}(\lambda) = \frac{1}{M} \sum_{k=0}^{M-1} x^{(i)}(k) \exp(-j2\pi k\lambda/M), \quad \lambda = 0,1,\dots,M/2$$

$$i = 1,2,\dots,K.$$

(2.1.1-1)

3. In general,  $M = M_1 \times N_0$  where  $M_1$  is a positive integer (assumed odd number), that is,  $M_1 = 2L_1 + 1$ . Since  $M$  is even and  $M_1$  is odd, we compromise on the value of  $N_0$  (closest integer). Generate,

$$\hat{M}_n^{(i)}(\lambda_1, \dots, \lambda_{n-1}) = \frac{1}{\Delta_0^{n-1}} \sum_{k_1=-L_1}^{L_1} \dots \sum_{k_{n-1}=-L_1}^{L_1}$$

$$\cdot Y^{(i)}(\lambda_1 + k_1) \dots Y^{(i)}(\lambda_{n-1} + k_{n-1})$$

$$\cdot Y^{(i)*}(\lambda_1 + \dots + \lambda_{n-1} + k_1 + \dots + k_{n-1}),$$

(2.1.1-2)

for  $i = 1,2,\dots,K$ . For example, in the special case of the bispectrum where no averaging is performed, that is,  $M_1 = 1$ ,  $L_1 = 0$ , we have the triple product

$$\hat{M}_3^{(i)}(\lambda_1, \lambda_2) = \frac{1}{\Delta_0^2} Y^{(i)}(\lambda_1) Y^{(i)}(\lambda_2) Y^{(i)*}(\lambda_1 + \lambda_2)$$

(2.1.1-3)

Equation (2.1.1-2) gives the user the option of performing averaging over neighboring frequencies to reduce the bispectrum estimation variance.<sup>60</sup> The number of adjacent frequencies over which this averaging is to be performed is determined by the

parameter  $M_1 = 2L_1 + 1$  as  $M_1$  must always be odd so that the number of points in both directions ( $k_1$  and  $k_2$ ) parallel to the bispectrum axes will have a midpoint or median that will contain the averaged value from both directions as given in equation (2.1.1-2). For  $L_1 = 0$ ,  $M_1 = 1$  and we have no frequency averaging with equation (2.1.1-3) resulting and  $M = M_1 \times N_0 = N_0$ . For  $L_1 = 1$ ,  $M_1 = 3$  and equation (2.1.1-2) would reflect frequency averaging over three adjacent frequency points along both axes of the bispectrum with  $M_1 \times N_0 = 3N_0 = M$  with the DFT performed over  $M = 3N_0$  points for each segment. Thus, the desired number of frequency samples is attained as  $M/M_1 = N_0$ . At the outset of using the direct method we specify  $N_0$  which is typically some convenient value for FFT computation. If we also have the frequency averaging option available to us then we can specify a value for  $M_1$  defining our averaging interval length along both bispectrum axes. This changes our original value of  $N_0$  which now becomes  $N_0/M_1 = M/M_1$  which is our new or effective value of  $N_0$  reflecting the frequency averaging, i.e., effective  $N_0 < \text{original } N_0$ . Since  $M_1$  is even and  $M$  is odd, the new value of  $N_0$  is usually not an integer. We compromise by choosing the closest integer to it which is used in the calculation of the scaling parameter for equation (2.1.1-2). The averaging operation does indeed reduce the variance but it may also introduce bias.<sup>60</sup> This brute force frequency averaging operation is implemented in Hi-Spec's direct bispectrum estimation routine "bispec\_d"<sup>1</sup> via a 2-D convolution of a frequency domain smoothing window with an averaged bispectrum over  $K$  segments (records) which is defined next.

4. The moment spectrum of the given data is the average over the  $K$  segments

$$\hat{M}_n^x(\omega_1, \dots, \omega_{n-1}) = \frac{1}{K} \sum_{l=1}^K M_n^{(l)}(\omega_1, \dots, \omega_{n-1}) \quad (2.1.1-4)$$

where  $\omega_i = (2\pi f_i / N_s) \lambda_r$

An optimal frequency domain smoothing window in the mean square error sense (MSE), the Rao-Gabr window<sup>14</sup> which optimizes the tradeoff between variance reduction and bias introduction, is offered as a Hi-Spec option. The Hi-Spec window implementation is defined as follows:<sup>1</sup>

1. The parameter *wind* specifies the frequency-domain smoothing window. If *wind* is a scalar, the Rao-Gabr window of length *wind* will be used. This window is defined by,<sup>14</sup>

$$W(m, n) = \frac{\sqrt{3}}{\pi^3} \left[ 1 - \frac{m^2 + n^2 + mn}{N^2} \right], (m, n) \in G$$

where  $N$  is half the FFT length,  $nfft$ , and  $G$  is the set of points,  $(m, n)$ , satisfying the ellipse

$$m^2 + n^2 + mn \leq \frac{wind^2}{(nfft/2)^2}$$

2. A unity value for *wind* results in no windowing.
3. If *wind*  $\leq 0$ , the default value of 5 will be used.

4. If *wind* is a vector, it is assumed to specify a 1-D window from which a 2-D window is computed,  $W(m,n) = w(m)w(n)w(m+n)$ .
5. If *wind* is a 2-D matrix, it is assumed to specify the 2-D smoother directly.

The net effect of this windowing procedure for steps 1 and 3 is that all of the points  $G$ , the shaded hexagonal region in Figure 2.1.1-1 from Rao<sup>14</sup> comprising the 12 symmetry regions of the bispectrum (see Appendix B) bounded by the ellipse area  $G_1$ , are windowed where  $G_1$  is the ellipse area

$$(m,n): \quad m^2 + n^2 + mn \leq \frac{wind^2}{(nff/2)^2},$$

$G$  is the shaded hexagonal area

$$(m,n): \quad |m| + |n| + |m+n| \leq 2 \frac{wind}{(nff/2)},$$

and  $G < G_1$ .

The optimal Rao-Gabr window reflects the minimization of the MSE consisting of the variance of the bispectral estimate plus the square of its bias. This weight function is actually an expression contained in the variance of the estimate and is shown to be smaller than any other bispectral weight function, thereby minimizing the MSE.<sup>14</sup>

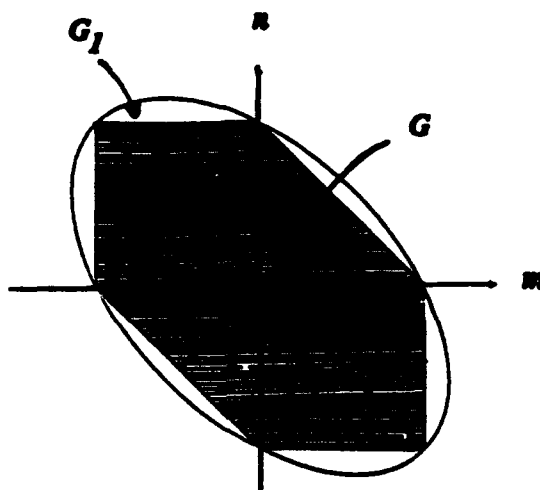


**Figure 2.1.1-1 Rao-Gabr Window Bounds**

### **2.1.1.1 Test Results**

As described in Appendix C synthetic signals at varying signal-to-noise ratios were generated to exercise the direct bispectrum algorithm. Results for synthetic signals embedded in Gaussian white noise indicate no significant improvement in bispectral analysis over power spectral analysis. The reason for this is that the signals simulated exhibited a symmetric pdf

(skewness approx. 0) which made it difficult for the algorithm to differentiate between non-Gaussian symmetric signals and non-Gaussian symmetric noise. Both of these are equally suppressed as the basic assumptions in regard to bispectral analysis are that the signals are non-Gaussian, zero-mean with non-zero skewness, i.e., exhibit non-symmetry, and that the noise is zero-mean Gaussian or non-Gaussian symmetric.

Real active sonar field data was processed with similar results to the simulated data for similar reasons, i.e., the projected signals used for pinging exhibit symmetric pdfs which were unperturbed upon backscattering from a target.

In summary, the results indicate that bispectral techniques which suppress Gaussian (or non-Gaussian - symmetric pdf) noise suffer from a lack of signal skewness which precludes any discernable improvement over power detection methods (see section C.2 of Appendix C).

### 2.1.2 Indirect Method

This class of conventional estimator is based on the 2-D FFT of a windowed third order cumulant function and is defined in Nikias<sup>16</sup> as follows.

Let  $\{X(1), X(2), \dots, X(N)\}$  be given data set. Then we have the following.

1. Segment the data into  $K$  records of  $M$  samples each, that is,  $N = KM$ .
2. Subtract the average value of each record.
3. Assuming that  $\{x^{(j)}(k), k = 0, 1, \dots, M-1\}$  is the data set per segment  $j = 1, 2, \dots, K$ , obtain estimates of the higher-order moments
4. Average over all segments
5. Generate the  $n$ th-order cumulant sequence  $\ell_n^x(\tau_1, \dots, \tau_{n-1})$ ; it is a function of

$$m_n^{(0)}(\tau_1, \dots, \tau_{n-1}) = \frac{1}{M} \sum_{k=S_1}^{S_2} x^{(0)}(k) x^{(0)}(k+\tau_1) \dots x^{(0)}(k+\tau_{n-1})$$

$$n = 2, 3, \dots, N; \quad i = 1, 2, \dots, K, \quad (2.1.2-1)$$

$$S_1 = \max(0, -\tau_1, \dots, -\tau_{n-1}),$$

$$S_2 = \min(M-1, M-1-\tau_1, M-1-\tau_2, \dots, M-1-\tau_{n-1}).$$

$$\hat{m}_n^x(\tau_1, \dots, \tau_{n-1}) = \frac{1}{K} \sum_{i=1}^K m_n^{(0)}(\tau_1, \dots, \tau_{n-1})$$

$$n = 2, 3, \dots, N-1. \quad (2.1.2-2)$$

moments from order second to  $n$ th (see Rosenblatt<sup>18</sup> for general relationship).

However, for a zero-mean process we have

$$\hat{c}_2^x(\tau) = \hat{m}_2^x(\tau)$$

$$\hat{c}_3^x(\tau_1, \tau_2) = \hat{m}_3^x(\tau_1, \tau_2)$$

and

$$\hat{c}_4^x(\tau_1, \tau_2, \tau_3) = \hat{m}_4^x(\tau_1, \tau_2, \tau_3) - \hat{m}_2^x(\tau_1) \hat{m}_2^x(\tau_3 - \tau_2)$$

$$- \hat{m}_2^x(\tau_2) \hat{m}_2^x(\tau_3 - \tau_1) - \hat{m}_2^x(\tau_3) \hat{m}_2^x(\tau_2 - \tau_1). \quad (2.1.2-3)$$

#### 6. Generate the higher-order spectrum estimate

$$\hat{C}_n^x(\omega_1, \dots, \omega_{n-1}) = \sum_{\tau_1=-L}^L \dots \sum_{\tau_{n-1}=-L}^L \hat{c}_n^x(\tau_1, \dots, \tau_{n-1})$$

$$(2.1.2-4)$$

$$\cdot W(\tau_1, \dots, \tau_{n-1}) \exp\{-j(\omega_1 \tau_1 + \dots + \omega_{n-1} \tau_{n-1})\},$$

where  $L < M - 1$  and  $W(\tau_1, \dots, \tau_{n-1})$  is a window function. Instead of a cumulant

spectrum, a moment spectrum can be generated by equation (2.1.2-4), if we substitute the

cumulants by moment estimates given by equation (2.1.2-2).

The multidimensional window function should satisfy the symmetry properties of higher-order moments or cumulants. They should also be zero outside the region of support of estimated cumulants and have nonnegative Fourier transforms. A class of functions that satisfies these constraints is the following.

$$W(\tau_1, \dots, \tau_{n-1}) = d(\tau_1)d(\tau_2)\dots d(\tau_{n-1})d(\tau_1 + \dots + \tau_{n-1}),$$

where

$$\begin{aligned} d(\tau) &= d(-\tau) \\ d(\tau) &= 0, \tau > L \\ d(0) &= 1 \end{aligned} \tag{2.1.2-5}$$

$$D(\omega) = \sum_{\tau=-L}^L d(\tau)\exp\{-j\omega\tau\} \geq 0, \text{ for all } \omega.$$

Identity (2.1.2-5) allows a reconstruction of window functions for higher-order spectrum estimation using standard one-dimensional  $(1 - d)$  windows. However, not all  $1 - d$  windows satisfy constraint  $D(\omega) \geq 0$  for all  $\omega$ . Two windows with good performance in terms of bias and variance minimization are (see Nikias<sup>15</sup> and references therein):

$$d_o(\tau) = \begin{cases} \frac{1}{\pi} \left| \sin \frac{\pi\tau}{L} \right| + \left(1 - \frac{|\tau|}{L}\right) \left(\cos \frac{\pi\tau}{L}\right), & |\tau| \leq L \\ 0, & |\tau| > L \end{cases} \tag{2.1.2-6}$$

and

$$d_p(\tau) = \begin{cases} 1 - 6\left(\frac{|\tau|}{L}\right)^2 + 6\left(\frac{|\tau|}{L}\right)^3, & |\tau| \leq \frac{L}{2} \\ 2\left(1 - \frac{|\tau|}{L}\right)^3, & \frac{L}{2} \leq |\tau| \leq L \\ 0, & |\tau| > L \end{cases} \quad (2.1.2-7)$$

The first window achieves a bias that is about 18 percent smaller than that of the second (Parzen) window. However, the first window produces variance that is about 26 percent larger than that of Parzen window. Equation (2.1.2-7) is applied in Hi-Spec to minimize the variance.

#### 2.1.2.1 Test Results

Conventional indirect bispectral analysis employing 2-D FFTs of higher order cumulants were examined for comparison with direct methods with the result that resolution was far superior using the direct algorithm (see section C.1 of Appendix C). The inability of the indirect bispectrum to: (1) resolve quadratic phase coupled components similarly to the direct bispectrum; and, (2) suppress uncoupled sinusoids mixed with coupled sinusoids; caused questions to be raised as to its effectiveness for noise suppression (uncoupled sinusoids should look like non-Gaussian symmetric pdf noise to the bispectrum). Thus, indirect bispectra comparison to power spectra was dropped pending a more detailed examination of the theory and implementation of conventional indirect bispectrum methods. (See section C.1 **DIRECT/INDIRECT BISPECTRUM COMPARISON FOR SIMULATED DATA.**)

## 2.2 PARAMETRIC METHODS

An alternative approach to Fourier based methods for the interpretation of time series data is the construction of white noise driven linear parametric models from the underlying physical process. The motivations for this are threefold: (1) to recover phase information accurately, (2) to increase the resolution capability of an estimator involving closely spaced peaks in the bispectrum domain, and (3) to increase bispectrum fidelity in the situations where non-Gaussian processes are actually parametric or may be approximated by parametric models.<sup>15</sup> These methods typically suffer in low signal-to-noise ratio environments and demand a certain amount of apriori knowledge which isn't always readily available in practice.

Parametric methods for higher-order spectrum estimation are described in section 7.4 of Nikias.<sup>16</sup> MA, noncausal AR, and ARMA methods are discussed respectively in relation to a nonminimum-phase system identification problem which stated simply is, given only a finite length of data, it is required to estimate the bispectrum of the underlying discrete random process via parametric modeling of its third moments.<sup>15</sup> For example, the MA method requires the estimation of the coefficients of the MA process via a typical second-order method to reflect the autocorrelation structure of the data. This apriori knowledge is then applied to the estimation process with the end result being a fine tuning to the coarse estimate made via the second-order process to improve resolution. A typical example of this in Hi-Spec is the "qpc\_tor" program defined under quadratic phase coupling in section A.0 of Appendix A.<sup>27</sup> This program uses a "third-order recursion" to estimate the bispectrum as a function of the AR model order which should be greater than the number of spectral lines, in particular, closely spaced spectral lines. The motivation for such parametric techniques is to (1) more accurately estimate bispectra of an AR process, and (2) resolve closely spaced peaks in the bispectrum or detect the presence or absence of quadratic phase coupling at frequency pairs in close

proximity to each other. The conjecture is made that, just as AR, ARMA models offer high resolution capabilities as alternatives to conventional power spectrum methods, their bispectral counterparts can be expected to offer similar high resolution capabilities compared to conventional direct or indirect bispectral estimators. Comparison examples are given in Raghuvveer.<sup>27</sup>

There appears to be some difference of opinion in the literature concerning the efficacy of assuming that a given time series can be described by a low order AR or ARMA model as reported in Thomson<sup>26</sup> which details the authors' experience in analyzing many different time series models from scientific and engineering problems with the statement that "neither of us has yet seen an example which could reasonably be described by an autoregressive model." This statement is later qualified by the admission that, while stating that such examples may exist, the probability of realizing one appears to be so low that "starting with the assumption that a given time series can be described by a low-order AR or ARMA model is a prescription for trouble." This is not the reason for neglecting parametric bispectral estimators in this paper as much as the requirement for the minimization of apriori knowledge in regard to bispectral signal detection versus second-order statistics power spectrum techniques, i.e., the main focus here is coarse as opposed to fine tuning although some alternative methods employing high-order statistics for resolution improvement will be listed in section 2.2.1.

### **2.2.1 Harmonic Retrieval Test Results**

As an adjunct to the problems encountered in bispectral signal detection due to the lack of echo or radiated signal skewness compared to noise contributions having negligible skewness, frequency resolution tests possible using the Hi-Spec routine "harm\_est" were performed using signals generated by "harm\_gen" (see Appendix A). The "harm\_est" routine

gives an estimation of the frequencies of real harmonics in noise with comparison to a conventional periodogram. The estimation is given using the MUSIC, Eigenvector, Pisarenko, ML (Capon) and AR methods based on the diagonal slice of fourth-order cumulants. No improvement was noted over nonparametric FFT-based direct bispectral algorithms as a FFT bispectral slice exhibited the same peak to peak response as the diagonal fourth-order cumulant slice. Moreover, for low signal-to-noise ratio cases, these higher-order statistical resolution improvement methods deteriorated significantly in comparison to the classic periodogram - a problem common to their second order counterparts.

It is noted that coarse adjustment (long range detection) as opposed to fine (target classification) is the main focus of this paper. It was the author's intent to call attention to the fact that higher-order methods are no resolution panacea. Lack of signal skewness inhibits any propagation gain as the signal is suppressed equally with the noise. Lack of sufficient SNR inhibits any resolution improvement. The latter is not a new result. The former verifies the examples from the literature review and the tests performed for this paper as reported in Appendix C.

## CHAPTER 3

### CONCLUSIONS/FUTURE WORK

This chapter examines the efficacy of signal detection in underwater acoustics using polyspectral methods in the light of current research into nonstationary HOS with future directions for study indicated.

#### 3.0 GENERAL CONCLUSION

The theme throughout this paper is that the critical parameter in relation to the third order cumulant spectrum (bispectrum) as defined in equation (B.2-5) successfully realizing any type of propagation gain over the second order cumulant spectrum (power spectrum) as defined in equation (B.2-3) is the signal skewness as defined in equation (B.1-6). Preliminary results, pending a more detailed examination of simulated/real data, indicate that if the echoed (active) or radiated (passive) signal does not exhibit a degree of moderate skewness which remains to be quantified, but as a rule of thumb approximately .5 where 1 indicates a highly skewed distribution, the probability that HOS signal processing sophistication will realize a significant detection improvement over second order methods appears to be low. This is borne out by observing that a time series representing a mixture of quadratically phase coupled sinusoids and uncoupled sinusoids exhibits a moderate skewness measure while a similar series representing only uncoupled sinusoids does not, i.e., suppression of the uncoupled sinusoids is realized in the former case while there is no difference between uncoupled sinusoids and Gaussian or non-Gaussian symmetric noise in the latter case.

### 3.1 NONSTATIONARY HIGHER-ORDER SPECTRA

Success in the area of nonstationary higher order spectral estimators resulting in a claimed 3 dB detection performance improvement under realistic conditions when compared to the stationary power spectrum has been reported in Wilson.<sup>29</sup> In this report the detection performance of different types of higher order spectra are discussed for a variety of signals. The introduction of what the authors refer to as a "new type of higher order spectra called nonstationary higher order spectra" is made with the distinction that these nonstationary higher order spectra are not stationary higher order spectra representations of nonstationary processes but rather are different spectra which contain the stationary higher order spectra as a subset of their domain. It is shown quantitatively through theoretical predictions and simulations that these spectra perform better at detecting nonstationary signals than do the traditional stationary spectra. The detection performance of the bispectrum is examined in comparison to the power spectrum. The motivation for the introduction of this new class of spectra is the detection of nonstationary signals such as harmonically related narrowband components of finite duration transients. A functional approach is used<sup>29</sup> to define the stationary higher order spectra or polyspectra and a statistical approach is used to define the nonstationary higher order spectra or cumulant spectra. The estimation of higher order spectra are discussed from both stationary and nonstationary perspectives.

The stationary functional approach defines a process with orthogonal increments based on the classical derivation as defined on page 32 of Priestly.<sup>50</sup> The nonstationary statistical approach assumes a vector valued discrete time series whose  $n$ th order cumulant exists and is finite. Then the  $n$ th order discrete Fourier transform of the cumulant exists and an  $n$ th order cumulant spectral density function is subsequently defined as the  $n$ th order discrete Fourier transform of the cumulant function. The key here is that no assumption of stationarity has

been made. For the estimation of nonstationary higher order spectra the result that the cumulant of the finite Fourier transforms is proportional to the  $n$ th order polyspectral density function plus lower order terms is extended to being proportional to the  $n$ th order cumulant spectral density function (defined above) plus lower order terms. The observation is made that, for stationary processes, the cumulant spectrum is zero except in the domain for which the sum of all frequency components are zero. Thus, within this domain the cumulant spectrum is equal to the classical polyspectrum defined by the stationary functional approach. (This domain is the dark shaded triangular region in the block labeled "1" in the first quadrant of Figure B.2-2 entitled, **Fundamental Domain of the Discrete Time Bispectrum**, from Section B.2. The light shaded triangular region adjacent to this domain becomes a region where non-zero values indicate nonstationarity.)

### 3.1.1 Conclusion

The bispectral results have previously been discussed in this paper (see Section 2.0). The message of the statistical approach taken in Wilson<sup>29</sup> is that blindly computing polyspectra is folly without taking the time to understand the underlying statistics of the processes involved which necessitates a certain degree of statistical preprocessing prior to attempting any type of polyspectral analysis. The nonstationary statistical approach used in the report to define cumulant spectral density functions lends itself to a better understanding of the statistics involved in polyspectral processing and is an example of the multidimensional statistical basis used for trispectrum (kurtosis) computations that will be addressed in section 3.2.

### 3.1.2 Future Work

Further examination is recommended to better understand the nuances between stationary and nonstationary higher order spectra computations from both algorithmic and interpretive viewpoints as a function of the underlying statistics (real and assumed) of the processes involved.

## 3.2 TRISPECTRUM

A natural extension to the bispectrum is the examination of fourth-order statistics (kurtosis) in reference to determining the degree of success for signal detection in the transform (trispectral) domains.<sup>35,36</sup> Work is specifically being directed toward computing the statistics for the trispectrum similar to that for the bispectrum<sup>29,31</sup> over the region of support in the first octant for trispectral computations, i.e., the principal domain of the trispectrum for stationary continuous time processes which is a triangular cone in the positive octant—the three sides of this cone being the planes formed by the intersections of three of the trispectrum's symmetry planes.<sup>36,49</sup>

As defined in (B.2-8) the trispectrum is the fourth order cumulant spectrum of a random process. The motivation for investigating the trispectrum as described further in Dalle Molle<sup>36</sup> is that bispectral tests don't serve as complete tests for the rejection of Gaussianity and linearity hypotheses. Although impractical, a complete test based on higher order spectra would involve all possible polyspectra as non-Gaussian processes may exist which have zero bispectral values and in turn zero skewness measure over the complete principal domain. It is observed that since most non-Gaussian processes have non-zero high order cumulants, it is unlikely that a process would have both its skewness and kurtosis functions identically equal to zero over the entire principal domain. Therefore, just as additional statistical goodness-of-fit

tests present stronger cases for acceptance/rejection of hypotheses, bispectral and trispectral based tests together make a stronger case for the rejection of the null hypothesis of Gaussianity. Similarly, the constancy of the skewness function is not always a good indicator for a linear model. Thus, the trispectrum presents a more powerful tool for the analysis of non-linear and non-Gaussian time series. For the trispectrum, the square of the average kurtosis function becomes the test for Gaussianity.<sup>36</sup> The symmetries which need to be considered in order to define the continuous and discrete time principal domains of the trispectrum along with the description of the wedge-shaped hyperplane cone in the frequency triple  $(f_1, f_2, f_3)$  which forms the continuous time principal domain are given in Dalle Molle.<sup>36</sup> This pyramid shaped wedge is defined explicitly for band limited processes. The principal domain of the trispectrum for a discrete time band limited process is derived in a similar manner to the bispectrum's principal domain. Sampling at the Nyquist frequency results in the discrete time principal domain being a pyramid with a triangular base that is larger than the support set for the continuous time band limited trispectrum.<sup>36</sup>

Kurtosis estimation has also been extensively addressed.<sup>38-48</sup> The occurrence of non-Gaussian signals in underwater acoustics due to multipath and modulation effects is the main motivation here as sinusoidal and narrowband Gaussian signals which, when propagated through fading or multipath environments, are received as non-Gaussian in terms of the frequency domain kurtosis estimate.<sup>38</sup> The results are applicable to both active and passive sonar with the active case conjectured to be non-Gaussian (skewness at the returns) due to modulation effects. Results have suggested the possibility of detecting non-Gaussian signals via kurtosis estimation at lower signal-to-noise ratios than the power spectrum method.

For under ice data the non-Gaussian signals are due to ice movement which produced transient and modulated signals in the passive case.<sup>38</sup> (If, in fact, sufficient skewness is

observed at the returns for the active case then third order statistics should generally discriminate between non-Gaussian and Gaussian signals.<sup>49)</sup> Kurtosis is defined to be the ratio of a fourth order central moment to the square of a second order central moment. It has been shown to be a locally optimum detection statistic under certain conditions and is extended in the frequency domain to the detection of outliers from an otherwise Gaussian sample - the outliers being equivalent to the randomly occurring signal that is to be detected.

Based on the analyses of real underwater acoustics data, conditions exist under which frequency domain kurtosis estimation indicates the presence of randomly occurring signals.<sup>39</sup> For a Gaussian distribution, kurtosis will have a value of around 3 within some bound as a function of the number of samples. For randomly occurring signals that produce non-Gaussian distributions, the kurtosis estimate can be less than or much greater than 3. A model for the received data which contained the effects of amplitude and phase fluctuation of the signal along with modulation effects was used to evaluate the kurtosis estimates in Dwyer.<sup>39</sup> The frequency domain kurtosis estimation was computed and shown to have significantly high values even for small signal-to-noise ratio cases surpassing the averaged power spectrum estimation in some instances due to its sensitivity to the pdf of the signal. Results from Dwyer<sup>39</sup> suggest that for randomly occurring signals, e.g., a transient or a modulated signal over long integration times, the frequency domain kurtosis estimate may be a better detection statistic than the power spectrum estimate. For fading environments which frequently occur in underwater acoustics, the kurtosis estimates are significantly enhanced.

The utility of the fourth order spectrum for the classification of transient signals in passive sonar and resonances in active sonar along with the computational drawbacks is given in Dwyer.<sup>43</sup> The importance of this is obvious because many noise sources, i.e., ambient, reverberation, flow, etc., are Gaussian compared to signals, i.e., sinusoids, transients, active

sonar transmissions, which are all non-Gaussian. It is demonstrated that the fourth order spectrum differentiates between a sum of sinusoids and thus can aid in active sonar classification. When long pulse trains are transmitted the return echo is usually modulated from target dynamics, Doppler spreading, or medium effects. Under these conditions the spectrum can be severely distorted making detection and classification impossible. Using an amplitude coded pulse train it is shown that the fourth order spectrum can extract range and Doppler information while for the same conditions the spectrum is useless.<sup>43</sup> The emphasis is on the special case of the fourth order cumulant defined as kurtosis in (B.1-6). The treatment here is multidimensional as a new class of non-Gaussian density functions which represent meaningful signals (independent data are not required) is introduced with their corresponding fourth order spectra. The importance of this work is related to the statistical treatment of modulated processes as related to sonar, in particular active sonar.

To demonstrate theoretical results in regard to frequency domain kurtosis estimation an experiment was conducted<sup>44</sup> where a sinusoid was modulated by white Gaussian noise, transmitted through the water and received on an omni-directional hydrophone. This was an attempt at simulating the modulation due to target effects which was previously discussed. The second order spectrum (power spectrum), the spectrum of the special case of the fourth order moment, and the spectrum of the special case of the fourth order cumulant (trispectrum) derived at the output of a lowpass filter were estimated from the filtered data. The experiment verified theoretical results by showing that the second order spectrum could not extract the sinusoidal frequency, but the respective spectrums of the fourth order moment and cumulant could. It is further reported<sup>44</sup> that the analysis of sonar data clearly show modulated or fluctuating signals. As the range increases between a source and receiver these fluctuating

components dominate the signal. This fluctuation was the reason for the Gaussian modulation of the transmitted signal in the experiment.

The properties of the special case of a fourth order cumulant are considered via implementation using 1-D Fourier transforms as opposed to the computational complexity involved with full 3-D Fourier transform realizations of the trispectrum as defined in (B.2-8). The derivation of the Fourier transform of the special case of a fourth order cumulant for the extraction of range and Doppler information is given in Dwyer.<sup>41,47</sup> An improvement on the order of that noted in Dwyer<sup>44</sup> for the detection of sinusoids was similarly observed when comparing fourth order cumulant techniques to the second order spectrum for range/Doppler applications. It was demonstrated by simulations that the Fourier transform of a special case of the fourth order cumulant could extract range and Doppler information with high resolution even when Gaussian noise was added to the echo while, under the same conditions, the ambiguity function and second order spectrum processing showed significant Doppler spreading losses.

### 3.2.1 Conclusion

It is recognized that the additional computational, statistical, and physical meaning complexity concomitant with trispectral computations may be the deciding factors in any kind of a tradeoff with a conjectured improvement over polyspectral methods of lower order.

### 3.2.2 Future Work

If special cases of fourth order cumulant spectrum (trispectrum) computations can be realized which minimize the computational effort required for otherwise full trispectrum realizations then the efforts cited above merit further scrutiny in regard to, at the very least,

signal classification which exploits the phase interactions of higher order statistics, and signal detection per se in comparison to second order methods. Abbreviated kurtosis estimation algorithms might even present viable alternatives to third order methods when signal skewness is not a problem, i.e., sufficient skewness exists to employ bispectral techniques. This did not appear to be the case, however for the real test data examined in this report as signal skewness, specifically lack of same, presented a very real problem in regard to the assumptions necessary for successful application of higher order spectra for detection purposes.

Dwyer's work points out the fact that power spectrum density (PSD) estimation is essentially a second order measure which is not sensitive to the statistical nature of the signals.<sup>38-48</sup> He offers, as an alternative, simple fourth order moment (kurtosis) tests in both frequency and time as supplements to PSD estimates and, in some cases of practical importance, as superior detection statistics to PSD techniques. It is highly recommended that the success which dwyer achieved using frequency domain kurtosis methods be extended to the time domain, as he suggests, for both active and passive sonar scenarios. Dwyer emphasizes that the time domain is nothing more than a special case of the frequency domain and that analogous results should also hold in the spatial domain where kurtosis methods could be evaluated in regard to target angle estimation. His past success, for low input signal-to-noise ratio cases (SNRi) using kurtosis methods exclusive of any cumulant connotations where kurtosis methods detected non-Gaussian signals while PSD methods failed to do so, is reason enough to verify his conjectures in both time and spatial domains.

Following Dwyer's lead, algorithms need to be developed which examine both the real and imaginary parts of the input data and optimally select the part or post processing of both parts which gives the best detection statistic as a function of: (1) the signal set used, (2) the target aspect angle, and (3) the kurtosis window length which defines a sliding kurtosis

window across an acoustic cycle (ping in active case, listening interval in passive case). The algorithms need to be examined in regard to: (1) edge effects resulting from the windowing procedure for simulated high and low kurtosis signals, specifically, how edge effects can maximize detection by dictating whether high or low kurtosis is sought for the detection statistic; (2) the effect of inducing high or low kurtosis to a signal distribution prior to pinging for the active case, specifically, how such inducement effects the signal upon backscattering from a target with particular attention paid to the degree of kurtosis observed post target dynamics and/or modulation effects; (3) evaluation against simulated test beds containing realistic targets from widely accepted sonar models as a function of target aspect, platform and target speed, turn rate, depth, position, and sea depth for fine tuning purposes, and finally, (4) exhaustive testing against as much real data as possible to verify or disprove Dwyer's conjectures, specifically, what signals are optimal for kurtosis as an effective detection statistic in the active case, and what kurtosis window lengths and post processing are optimal in the passive case. The utility of kurtosis for detection would then have to be compared with standard second order methods in a ROC curve sense for quantification purposes.

It is worth noting that work has begun on an algorithm, Induced Kurtosis Statistic Anomaly Detector (IKSAD),<sup>53</sup> to test Dwyer's conjectures with the initial results being very encouraging. The algorithm, currently in development is a sliding windowed kurtosis in time over an acoustic cycle. Tests were performed using simulated data generated by the Target Echo, Noise, and Reverberation (TENAR) Model.<sup>54</sup> The results, for a wide selection of platform and target dynamic parameters in shallow water scenarios at varying target aspects, indicate successful target location as an extrema over the acoustic cycle in almost 80% of the cases without any type of signal post processing for a complete range of SNR<sub>i</sub> = 15 dB down to -15 dB in decrements of 5 dB. The algorithm uses no FFTs and, as such, is independent of

doppler. It merely uses a normalized simple fourth order moment (kurtosis) as a detection statistic to exploit the active signal perturbation upon backscattering as a function of target dynamics and/or modulation effects suggested by Dwyer. In short, it is concerned only with the statistical distribution of the echoed signal over the target extent. Additional simulated tests against specific targets of interest at aspects of interest for both shallow water and deep ocean scenarios were performed with a high degree of success, upward of 90%, in the SNRi range of [15,-15] dB. All simulated tests utilized a 15 degree beam at a look angle of 0 degrees, i.e., directly on the Main response Axis (MRA). Preliminary tests against real data (static and dynamic) have also been performed with the algorithm again achieving success in the SNRi = [15,-15] dB range for abbreviated test sets. More real data needs to be analyzed to thoroughly exercise IKSAD over a trial set comprising the most probable scenarios which will be encountered. This is necessary to complete the evaluation of Dwyer's conjectures.

The TENAR model,<sup>54</sup> used for the generation of simulated data, predicts the levels and complex cross-correlations of sound "heard" by a multichannel active or passive sonar system in a specified environment. Sound sources may include ambient noise, target radiated noise, sonar self noise, target echoes and reverberation (surface, volume, and bottom). Two propagation models are offered: isovelocity (straight line) with boundary reflections, or Weinberg's CONGRATS ray tracing.<sup>57</sup> Eggan and Goddard developed the sequence of programs for generating TENAR's simulated multichannel reverberation.<sup>54</sup> These programs are further described in broad outline form by Luby<sup>55</sup> with the physical and mathematical background given by Princehouse.<sup>56</sup>

This reverberation capability has now been integrated into The Sonar Simulation Toolset (SST)<sup>58</sup> developed with sponsorship from several U. S. Navy sources including the Applied Research Laboratory of The Pennsylvania State University (Lee Culver, Leon Sibul,

and Frank Symons, Jr.). SST is a set of computer programs, input files, object-oriented software components, and software development tools for building and running sonar simulations. In this context, a "sonar simulation" is a computer-based process for predicting the response of a sonar system to a particular environment. It produces a digital representation of the predicted signal in each channel of the sonar receiver's processing path. This signal includes random fluctuations with the correct statistical properties. The SST enables a user to create an "artificial ocean" for: (1) testing new or proposed sonar systems or tactics, (2) training sonar operators, (3) planning experiments, or (4) validating models of underwater acoustic phenomena by comparing simulation results with measurements. Inputs to a sonar simulation include: (1) the characteristics of the ocean itself (sound propagation, sound scattering, ambient noise), (2) active targets (scatterers of an active sonar's pulses), (3) passive targets (noise sources), (4) the sonar transmitter (pulses, beams, trajectory), and (5) the sonar receiver (beams, trajectory, signal processing, self noise). SST commands available now can generate reverberation and target echoes for a multichannel active sonar and compute the signal received by a multichannel passive sonar from any number of maneuvering sources. Three different methods for generating reverberation are: (1) random point scatterer based, (2) Gaussian integration, or (3) Monte Carlo integration. A straight line (isovelocity) sound propagation model is built in; alternatively, the user may choose a propagation model based on eigenray files produced by NUWC's Generic Sonar Model (GSM). The latter mechanism makes all five of GSM's propagation models available to the SST. The scattering function produced using the Gaussian and Monte Carlo integrations is a time dependent cross spectral density matrix for reverberation. SST uses this scattering function to produce a multichannel stochastic time series for subsequent analysis.<sup>58</sup>

It is the author's intent to use SST, in particular SST's ability to reflect the correct statistical properties of the received signal for a specified environment, to quantify his work with IKSAD<sup>53</sup> in relation to current detection methods. The final result will be a qualification of Dwyer's conjectures regarding the utility of time domain kurtosis as an effective detection statistic for both active and passive sonars.

## REFERENCES

1. ***Hi-Spec Software Reference Manual For Signal Processing With Higher-Order Spectra - Version 1.0***, United Signals & Systems, Inc., Culver City, CA, 1991.
2. C. L. Nikias, J. M. Mendel, ***Signal Processing With Higher-Order Spectra***, United Signals & Systems, Inc., Culver City, CA 1990.
3. M. H. Kauderer, M. F. Becker, E. J. Powers, "Acoustical Bispectral Processing," ***Applied Optics***, Vol. 28, No. 3, pp. 627-637, 1 February 1989.
4. A. Petropulu, C. L. Nikias, "Analytic Performance Evaluation of the Bicepstrum," ***ICASSP-89***, Vol. 4, pp. 2337-2340, Glasgow, Scotland, IEEE, Piscataway, NJ, 1989.
5. D. Lagoutte, F. Lefeuvre, "Application of Bicoherence Analysis in Study of Wave Interactions in Space Plasma," ***J. of Geophysical Research***, Vol. 94, No. A1, pp. 435-442, 1 January 1989.
6. M. J. Hinich, C. S. Clay, "The Application of the Discrete Fourier Transform in the Estimation of Power Spectra, Coherence, and Bispectra of Geophysical Data," ***Reviews of Geophysics***, Vol. 6, No. 3, pp. 347-363, August 1968.
7. E. J. Powers, R. W. Miksad, "Applications of Frequency and Wavenumber Nonlinear Digital Signal Processing to Nonlinear Hydrodynamics Research," Contract N00167-88-K-0049, Office of Naval Research, Applied Hydrodynamics Research (AHR) Program, 14 pages, 18 December 1989.
8. C. L. Nikias, R. Pan, "ARMA Modeling of Fourth-Order Cumulants and Phase Estimation," Contract No. ONR-N000114-86-K-0219, Office of Naval Research, 25 July 1987.

## REFERENCES (Continued)

9. R. F. Dwyer, "Asymptotic Detection Performance of Discrete Power and Higher-Order Spectra Estimates," *IEEE J. of Oceanic Engineering*, Vol. OE-10, No. 3, pp. 303-315, July 1985.
10. S. Bellini, B. Rocca, "Asymptotically Efficient Blind Deconvolution," *Signal Processing*, Vol. 20, pp. 193-209, July 1990.
11. H. Abarbanel, R. Davis, G. J. MacDonald, W. Munk, "Bispectra," Report No. JSR-83-204, The Mitre Corporation, McClean, VA, 76 pages, January 1985.
12. *PRO-MATLAB*, The MathWorks, Inc., South Natick, MA, 1 January 1991.
13. *Signal Processing Toolbox*, The MathWorks, Inc., South Natick, MA, August 1988.
14. T. Subba Rao, M. Gabr, *An Introduction to Bispectral Analysis and Bilinear Time-Series Models*, pp. 42-43, Springer-Verlag, New York 1984.
15. C. L. Nikias, M. R. Raghuveer, "Bispectrum Estimation, A Digital Signal Processing Framework," *Proc. IEEE*, Vol. 75, pp. 869-891, July 1987.
16. C. L. Nikias, "Higher-Order Spectral Analysis," *Advances in Spectrum Analysis and Array Processing - Volume I*, S. Haykin, editor, pp. 326-365, Prentice-Hall, Inc., Englewood Cliffs, NJ, 1991.
17. M. J. Hinich, "Testing for Gaussianity and Linearity of a Stationary Time Series," *J. Time Series Analysis*, Vol. 3, pp. 169-176, 1982.
18. M. Rosenblatt, *Stationary Sequences and Random Fields*, Birkhauser, Boston, 1985.
19. R. Pan, C. L. Nikias, "Harmonic Decomposition Methods in Cumulant Domains," *Proc. IEEE ICASSP-88*, pp. 2356-59, New York, 1988.

## REFERENCES (Continued)

20. A. Swami, J. M. Mendel, "Cumulant-based Approach to the Harmonic Retrieval and Related Problems," *IEEE Trans. ASSP*, Vol. 39, pp. 1099-1109, May 1991.
21. J. A. Cadzow, "Spectral Estimation: An Overdetermined Rational Model Equation Approach," *Proc. IEEE*, Vol. 70, pp. 907-938, 1982.
22. C. R. Baker, A. F. Gualtierotti, "Likelihood Ratios and Signal Detection for Non-Gaussian Processes," pp. 154-180, Chapter 6, *Stochastic Processes in Underwater Acoustics*, Edited by C. R. Baker, Lecture Notes in Control and Information Sciences, Vol. 85, Springer-Verlag, Berlin, 1986.
23. I. Jouny, E. K. Walton, R. L. Moses, F. D. Garber, "Bispectral Analysis of Radar Signals with Application to Target Classification," Report No. 723090-2, The Ohio State University ElectroScience Laboratory, Columbus, OH, 199 pages, August 1990.
24. P. S. Allison, "Bispectral Inversion: The Construction of a Time Series from its Bispectrum," Report No. ARL-TR-88-19, Applied Research Laboratories, U. of Texas, Austin, TX, 97 pages, April 4, 1988.
25. E. Dilaveroglu, M. A. Wickert, "Biperiodogram Frequency Estimates: Asymptotic and Finite Sample Size," *ICASSP-92*, Vol. 5, pp. 217-220, San Francisco, CA, IEEE, Piscataway, NJ, 1992.
26. D. J. Thomson, A. D. Chave, "Jackknifed Error Estimates for Spectra, Coherences, and Transfer Functions," *Advances in Spectrum Analysis and Array Processing - Volume I*, S. Haykin, editor, pp. 58-113, Prentice-Hall, Inc., Englewood Cliffs, NJ, 1991.
27. M. R. Raghuveer, C. L. Nikias, "Bispectrum Estimation: A Parametric Approach," *IEEE Trans. ASSP*, Vol. 33, pp. 1213-1230, October 1985.

## REFERENCES (Continued)

28. A. A. Giordano, F. M. Hsu, *Least Square Estimation with Applications to Digital Signal Processing*, John Wiley & Sons, New York, NY, 1985.
29. G. R. Wilson, K. R. Hardwicke, "Nonstationary Higher Order Spectral Analysis," Report No. ARL-TR-91-8, Applied Research Laboratories, U. of Texas, Austin, TX, 70 pages, April 23, 1991.
30. G. R. Wilson, M. L. Bartlett, K. R. Hardwicke, "Detection of Linear Periodically Time Varying Processes Using Higher Order Spectra," International Signal Processing Workshop on Higher Order Statistics, 4 pages, Chamrousse, France, July 10-12, 1991.
31. M. J. Hinich, G. R. Wilson, "Detection of Non-Gaussian Signals in Non-Gaussian Noise Using the Bispectrum," *IEEE Trans. on ASSP*, Vol. 38, No. 7, pp. 1126-1131, July 1990.
32. M. J. Hinich, "Detecting a Transient Signal by Bispectral Analysis," *IEEE Trans. on ASSP*, Vol. 38, No. 7, pp. 1277-1283, July 1990.
33. M. J. Hinich, G. R. Wilson, "Time Delay Estimation Using the Cross-Bispectrum," Proc. Oceans '90 Conference, 9 pages, Washington, D.C., September 24-26, 1990.
34. J. W. Dalle Molle, M. J. Hinich, "Cumulant Spectra-Based Tests for the Detection of a Coherent Signal in Noise," International Signal Processing Workshop on Higher Order Statistics, 3 pages, Chamrousse, France, July 10-12, 1991.
35. C. L. Nikias, "Parametric Trispectrum Estimation," Proc. IEEE 3rd ASSP Workshop on Spectrum Estimation and Modeling, pp. 17-20, Boston, MA, Nov. 17-18, 1987.

## REFERENCES (Continued)

36. J. W. Dalle Molle, M. J. Hinich, "The Trispectrum," Workshop on Higher-Order Spectral Analysis, sponsored by the ONR and NSF in cooperation with the IEEE Societies: ASSP, Control Systems, and Geoscience and Remote Sensing, pp. 68-72, Vail, CO, June 28-30, 1989.
37. G. R. Wilson, "Detection and Time Delay Estimation of Non-Gaussian Signals in Noise," Report No. ARL-TR-90-25, Applied Research Laboratories, U. of Texas, Austin, TX, 91 pages, July 31, 1990.
38. R. F. Dwyer, "Detection of Randomly Occurring Signals Using Spectra and Frequency Domain Kurtosis Estimates." Technical Memorandum TM No. 841057, NUSC, New London, CT, 58 pages, March 23, 1984.
39. R. F. Dwyer, "Use of the Kurtosis Statistic in the Frequency Domain as an Aid in Detecting Random Signals," IEEE J. of Oceanic Engineering, Vol. 9, No. 2, pp. 85-92, April 1984.
40. R. F. Dwyer, "Asymptotic Detection Performance of Discrete Power and Higher-Order Spectra Estimates," IEEE Journal of Oceanic Engineering, Vol. 10, No. 3, pp. 303-315, July 1985.
41. R. F. Dwyer, "The Extraction of Range and Doppler from Fourth-Order Spectra," ICASSP 90, Vol. 5, pp. 2403-2379, Albuquerque, NM, 3-6 April 1990.
42. R. F. Dwyer, "Fourth-Order Spectra of Mixture Processes," ICASSP 89, Vol. 4, pp. 2333-2336, Glasgow, Scotland, 23-26 May 1989.
43. R. F. Dwyer, "Fourth-Order Spectra of Mixture and Modulated Processes," Report No. TR-8403, NUSC, New London, CT, 27 pages, October 6, 1988.

## REFERENCES (Continued)

44. R. F. Dwyer, "Fourth-Order Spectra of Gaussian Amplitude-Modulated Sinusoids," *J. Acoust. Soc. Am.*, Vol. 90, No. 2, Pt. 1, pp. 918-926, August 1991.
45. R. F. Dwyer, "Detection of non-Gaussian Signals by Frequency Domain Kurtosis Estimation," *Proc. ICASSP '83*, Vol 2, pp. 607-610, April 1983.
46. R. F. Dwyer, "High-Order Spectra of Mixture Processes," Fourth Annual ASSP Workshop on Spectrum Estimation and Modeling, Presentation Summary, page 186, Aug 3-5, 1988.
47. R. F. Dwyer, "Range and Doppler Information from Fourth-Order Spectra," *IEEE J. of Oceanic Engineering*, Vol. 16, No. 3, 11 pages, July 1991.
48. R. F. Dwyer, "Fourth-Order Spectra of Sonar Signals," Workshop on Higher-Order Spectral Analysis, sponsored by the ONR and NSF in cooperation with the IEEE Societies: ASSP, Control Systems, and Geoscience and Remote Sensing, pp. 52-55, Vail, CO, June 28-30, 1989.
49. M. J. Hinich, Personal Correspondence, January/February 1992.
50. M. B. Priestley, *Non-Linear and Non-Stationary Time Series Analysis*, Academic Press, New York, 1988.
51. A. W. Lohmann, B. Wimitzer, "Triple Correlations," Physikalisches Institut der Universitat Erlangen-Nurnberg, 13 pages, D8520 Erlangen, Germany.
52. W. H. Press, B. P. Flannery, S. A. Teukolsky, W. T. Vetterling, *Numerical Recipes*, Cambridge University Press, Cambridge, 1989.

**REFERENCES (Continued)**

53. G. L. Morella, **Induced Kurtosis Statistic Anomaly Detector (IKSAD)**, VAX 9210 PRO-MATLAB program, developed October, 1992, modified February, 1993, Applied Research Laboratory, The Pennsylvania State University.
54. C. J. Eggen, R. P. Goddard, **TENAR User's Manual Version 3**, Applied Physics Laboratory, College of Ocean and Fisheries Sciences, University of Washington, Seattle, WA, January 1989.
55. J. C. Luby, "A New Reverberation Simulation Capability," APL-UW TM 1-87, Applied Physics Laboratory, University of Washington, Seattle, WA 1987.
56. D. W. Princehouse, "Reverberation generator Ocean Algorithm, A Status Report," APL-UW 7806, Applied Physics Laboratory, University of Washington, Seattle, WA, 1978.
57. H. Weinberg, "A Continuous Gradient Ray Tracing Technique for Acoustic Ray Analysis," *J. Acoust. Soc. Am.*, Vol. 50, No. 3, Pt. 2, pp. 975-984, September 1971.
58. R. P. Goddard, **Sonar Simulation Toolset User's Manual**, APL-UW TR 8908, Release 2.6, Applied Physics Laboratory, University of Washington, Seattle, WA, August 1992.
59. I. I. Jouny, R. L. Moses, "The Bispectrum of Complex Signals: Definitions and Properties," *IEEE Trans. on Signal Processing*, Vol. 40, No. 11, pp. 2833-2836, November 1992.
60. D. Kletter, H. Messer, "Suboptimal Detection of Non-Gaussian Signals by Third-Order Spectral Analysis," *IEEE Trans. on ASSP*, Vol. 38, No. 6, pp. 901-909, June 1990.

**APPENDIX A**

**HI-SPEC**

## A.0 SOFTWARE DESCRIPTION

A brief description of Hi-Spec Routines follows<sup>1</sup>.

### Higher-Order Spectrum Estimation: Conventional Methods

|                 |   |
|-----------------|---|
| <b>cum_est</b>  | Computes sample estimates of cumulants                            |
| <b>bispec_d</b> | Direct method for bispectrum estimation                           |
| <b>bispec_i</b> | Indirect method for bispectrum estimation                         |
| <b>gl_stat</b>  | Detection statistics for Hinich's Gaussianity and Linearity tests |

### Higher-Order Spectrum Estimation: Parametric Methods

|                 |  |
|-----------------|--|
| <b>cum_true</b> | Computes theoretical (true) cumulants of AR, MA and ARMA processes |
| <b>rp_iid</b>   | Generates sequence of i.i.d. random variables                      |
| <b>arma_syn</b> | Generates ARMA synthetics  |
| <b>ar_rcest</b> | Estimates AR parameters using correlation and/or cumulants         |
| <b>ma_est</b>   | Estimates MA parameters  |
| <b>arma_qs</b>  | Estimates AR parameters using the q-slice algorithm                |
| <b>arma_rts</b> | Estimates ARMA parameters using the residual time series method    |
| <b>tls</b>      | Total least squares solution to a set of linear equations          |

### Quadratic Phase Coupling

|                |   |
|----------------|---|
| <b>qpc_gen</b> | Generates quadratically phase-coupled harmonics in noise                |
| <b>qpc_tor</b> | Parametric QPC detection of quadratic phase coupling via the TOR method |

### Harmonic Retrieval

|                 |  |
|-----------------|--|
| <b>harm_gen</b> | Generates harmonics in Gaussian (colored) noise for the harmonic retrieval problem |
|-----------------|--|

**harm\_est** Estimation of power spectra of harmonics using MUSIC, Eigenvector, Pisarenko, ML (Capon) and AR methods based on the diagonal slice of the fourth-order cumulant with conventional periodogram also given for comparison purposes

#### Time-Delay Estimation

**tde\_gen** Generates Synthetics for time-delay estimation

**tde** Estimates time-delays from two sensor measurements using third order cross cumulants

#### Array Processing

**doa\_gen** Generates Synthetics for DOA problem

**doa** Estimates number of sources and their bearings from a linear array of sensors using MUSIC, eigenvector, Pisarenko, ML (Capon) and AR methods based on spatial fourth-order cumulants

#### Adaptive Linear Prediction

**riv\_dl** Adaptive LP using double lattice filter

**riv\_tr** Adaptive LP using transversal filter

**iv\_cal** Computes instrumental variable processes

#### Magnitude and Phase Retrieval

**biceps** Estimates impulse response via the bicepstrum method and computes complex cepstrum of a signal

**matul** Estimates Fourier Phase and magnitude of a signal using the Matsuoka-Ulrych algorithm

### Undocumented Functions

**cum2\_est** Estimates covariances  
**cum3\_est** Estimates third-order cumulants  
**cum4\_est** Estimates fourth-order cumulants

## A.1 BISPECTRUM ROUTINES

The bispectrum of the process,  $y$ , is estimated via the direct (FFT-based) and indirect methods.<sup>1,15</sup>

For the direct method, the time-series,  $y$ , is segmented into possibly overlapping records; the mean removed from each record, and the FFT computed; the bispectrum of the  $k$ -th record is computed as

$$B_k(m,n) = X_k(m)X_k(n)X_k^*(m+n), \quad (\text{A.1-1})$$

where  $X_k$  denotes the FFT of the  $k$ th record. The bispectral estimates are averaged across records, and an optional frequency-domain smoother (Rao-Gabr window)<sup>14</sup> is applied.

For the indirect method, the time-series,  $y$ , is again segmented into possibly overlapping records; unbiased sample estimates of third-order cumulants are computed for each record and then averaged across records; a Parzen lag window is applied to the estimated cumulants, and the bispectrum is obtained as the 2-D FFT of the windowed cumulant function.

## A.2 GAUSSIANTY TESTS

A decision statistic for Hinich's Gaussianity test is estimated.<sup>1</sup> The bispectrum is estimated using the direct method, and a frequency-domain 2-D boxcar smoother is applied. The power spectrum is estimated via the direct method, and a boxcar smoother is applied. The bicoherence is then estimated. The Gaussianity test (actually zero-skewness test) basically involves deciding whether or not the estimated bicoherence is zero.

The statistic for the Gaussianity test,  $sg$ , is a three-element vector where  $sg(1)$  is the estimated statistic  $S$ ,  $sg(2)$ , is the number of degrees of freedom,  $p$ , and the probability of false alarm,  $sg(3)$ , is the probability that a  $\chi^2$  random variable with  $p$  degrees of freedom could have a value larger than the estimated  $S$  in  $sg(1)$ . If this probability is small, say, 0.05, then we may reject the hypothesis of zero skewness at a PFA (or significance level) of 0.05. Therefore, if you decide to accept the hypothesis that the data have non-zero skewness, then the probability that the data may actually have zero skewness is given by  $sg(3)$ . If PFA is large, then the hypothesis of zero skewness cannot be easily rejected.

The normalized bispectrum (bicoherence) is defined as

$$B_n(\omega_1, \omega_2) = \frac{B(\omega_1, \omega_2)}{(S(\omega_1)S(\omega_2)S(\omega_1 + \omega_2))^{1/2}} \quad (\text{A.2-1})$$

where  $B_n(\omega_1, \omega_2)$  is the bispectrum and  $S(\omega)$  is the power spectrum. Under the Gaussianity (zero skewness) assumption, the expected value of  $B_n(\omega_1, \omega_2)$  is zero. The test of Gaussianity is based on the mean bicoherence power,

$$S = \sum |B_n(\omega_1, \omega_2)|^2, \quad (\text{A.2-2})$$

where the summation is performed over the non-redundant region as defined in Hinich.<sup>17</sup> The statistic  $S$  is  $\chi^2$  distributed, with  $p$  degrees of freedom, where  $p$  is a function of the FFT length and a resolution parameter,  $cparm$ ; <sup>17</sup>  $p$  is approximately equal to  $N^2/6M^2$ , where  $N$  is the length of the time series.

### A.3 HARMONIC ESTIMATION

Let  $C$  denote the *maxlag* by *maxlag* matrix, with entries,  $C(i,j) = C_{ij}(i - j, 0, 0)$ .

Also, let  $C = VSV'$  denote the eigenvector decomposition, where  $S$  is the diagonal matrix of eigenvalues,  $\lambda(k)$ , and  $V$  is the matrix of eigenvectors,  $v_k$ ,  $k = 1, \dots, \text{maxlag}$ . Let

$$e(\omega) := [1, \exp(-j\omega), \dots, \exp(-j(\text{maxlag} - 1)\omega)]' \quad (\text{A.3-1})$$

denote the FFT vector, and let  $p$  denote the chosen order (the parameter *p\_order*). Then, the cumulant-based power spectra are obtained as follows<sup>1</sup>.

$$P(\omega) = \left( \sum_{k=1}^M w(k) |e'(\omega)v_k|^2 \right)^{-1} \quad (\text{A.3-2})$$

where,

$$w(k) = \begin{cases} 1 & \text{MUSIC} \\ 1/\lambda(k) & \text{Eigenvector} \\ \delta(k - M) & \text{Pisarenko} \end{cases}$$

where  $\delta(k)$  is the Kronecker delta function.

The AR power spectrum is obtained as follows: First, a rank  $p$  approximation of the matrix  $C$  is obtained, as  $\hat{C} = VS\hat{V}'$ , where  $\hat{S}$  is obtained from  $S$  by setting  $\lambda_k = 0$ ,  $k = p+1, \dots, M$ .

The AR parameter vector is then obtained as the solution to  $\hat{C}a = 0$ ; the method in Cadzow<sup>21</sup> is used, and the solution is forced to have unity modulus.<sup>1</sup>

The ML(Capon) solution is given by,

$$P_{ML}(\omega) = \left( \sum_{k=1}^p \frac{1}{\lambda(k)} |e'(\omega)v_k|^2 \right)^{-1} \quad (\text{A.3-3})$$

**APPENDIX B**

**POLYSPECTRA THEORY**

## B.0 INTRODUCTION

This appendix presents an overview of the definitions, properties, and estimation methods of higher-order statistics or cumulants of stochastic signals and their associated Fourier transforms known as higher-order spectra or polyspectra as presented in the tutorial references. 2,15,16

## B.1 MOMENTS AND CUMULANTS

Higher-order spectra of stationary stochastic signals are defined in terms of cumulants and are referred to as cumulant spectra. Given a set of  $n$  real random variables

$\{x_1, x_2, \dots, x_n\}$ , their joint cumulants of order  $r = k_1 + k_2 + \dots + k_n$  are defined as

$$c_{k_1 \dots k_n} \triangleq (-j)^r \frac{\partial^r \ln \Phi(\omega_1, \omega_2, \dots, \omega_n)}{\partial \omega_1^{k_1} \partial \omega_2^{k_2} \dots \partial \omega_n^{k_n}} \Bigg|_{\omega_1 = \omega_2 = \dots = \omega_n = 0} \quad (\text{B.1-1})$$

where

$$\Phi(\omega_1, \omega_2, \dots, \omega_n) = E \{ \exp j(\omega_1 x_1 + \dots + \omega_n x_n) \} \quad (\text{B.1-2})$$

is their joint characteristic function. The joint moments of order  $r$  of the same set of random variables are given by

$$m_{k_1 \dots k_n} \triangleq E \{ x_1^{k_1} x_2^{k_2} \dots x_n^{k_n} \} = (-j)^r \frac{\partial^r \Phi(\omega_1, \omega_2, \dots, \omega_n)}{\partial \omega_1^{k_1} \dots \partial \omega_n^{k_n}} \Bigg|_{\omega_1 = \dots = \omega_n = 0} \quad (\text{B.1-3})$$

The joint cumulants can be expressed in terms of the joint moments of the set of random variables as follows for the moments  $m_1, m_2, m_3, m_4$ :

$$\begin{aligned} m_1 &= E(x_1) & m_2 &= E(x_1^2) \\ m_3 &= E(x_1^3) & m_4 &= E(x_1^4) \end{aligned}$$

of the random variable  $\{x_1\}$  are related to its cumulants by

$$\begin{aligned} c_1 &= m_1 \\ c_2 &= m_2 - m_1^2 \\ c_3 &= m_3 - 3m_2m_1 + 2m_1^3 \\ c_4 &= m_4 - 4m_3m_1 - 3m_2^2 + 12m_2m_1^2 - 6m_1^4. \end{aligned}$$

It is clear that the computation of the  $r$ th-order cumulant of  $\{x_1\}$  requires knowledge of all its moments from order first to  $r$ th, i.e.,  $m_1, m_2, \dots, m_r$ . If  $\{x(k)\}$ ,  $k = 0, \pm 1, \pm 2, \dots$  is a real, strictly stationary random process with zero mean,  $E(x(k)) = 0$ , then the moment sequences of the process are related to its cumulants as follows:

$$m_n^x(\tau_1, \tau_2, \dots, \tau_{n-1}) = \bar{E}\{x(k)x(k+\tau_1)\dots x(k+\tau_{n-1})\} \quad (\text{B.1-4})$$

where the moments up to order  $n$  exist and depend only on the time differences

$\tau_1, \tau_2, \dots, \tau_{n-1}$ . Taking into account the zero mean condition above, the cumulants are

related to the moments as follows for orders  $n = 1, 2, 3, 4$ :

$$c_1^x = m_1^x = E\{x(k)\} = 0 \quad (\text{mean value}), \quad (\text{B.1-5a})$$

$$c_2^x(\tau_1) = m_2^x(\tau_1) - m_1^{x^2} = m_2^x(\tau_1) = E\{x(k)x(k+\tau_1)\} \quad (\text{B.1-5b})$$

(covariance sequence),

where  $m_2^x(\tau_1)$  is the autocorrelation sequence,

$$c_3^x(\tau_1, \tau_2) = m_3^x(\tau_1, \tau_2) - m_1^x [m_2^x(\tau_1) + m_2^x(\tau_2) + m_2^x(\tau_2 - \tau_1)] + 2m_1^{x^3} \quad (\text{B.1-5c})$$

$$c_3^x(\tau_1, \tau_2) = m_3^x(\tau_1, \tau_2) = E\{x(k)x(k+\tau_1)x(k+\tau_2)\}$$

(third-order moment or cumulant sequence),

$$\begin{aligned} c_4^x(\tau_1, \tau_2, \tau_3) &= m_4^x(\tau_1, \tau_2, \tau_3) - m_2^x(\tau_1) \cdot m_2^x(\tau_3 - \tau_2) - m_2^x(\tau_2) \\ &\cdot m_2^x(\tau_3 - \tau_1) - m_2^x(\tau_3) \cdot m_2^x(\tau_2 - \tau_1) - m_1^x [m_3^x(\tau_2 - \tau_1, \tau_3 - \tau_1) \\ &+ m_3^x(\tau_2, \tau_3) + m_3^x(\tau_2, \tau_4) + m_3^x(\tau_1, \tau_2)] \\ &+ 2m_1^{x^2} [m_2^x(\tau_1) + m_2^x(\tau_2) + m_2^x(\tau_3) + m_2^x(\tau_3 - \tau_1) \\ &+ m_2^x(\tau_3 - \tau_2) + m_2^x(\tau_2 + \tau_1)] - 6m_1^{x^4}. \end{aligned}$$

(B.1-5d)

$$\begin{aligned}
c_4^x(\tau_1, \tau_2, \tau_3) &= m_4^x(\tau_1, \tau_2, \tau_3) - m_2^x(\tau_1) \cdot m_2^x(\tau_3 - \tau_2) - m_2^x(\tau_2) \\
&\cdot m_2^x(\tau_3 - \tau_1) - m_2^x(\tau_3) \cdot m_2^x(\tau_2 - \tau_1) \\
&= E\{x(k) x(k + \tau_1) x(k + \tau_2) x(k + \tau_3)\}
\end{aligned}$$

(fourth-order moment sequence).

Equations (B.1-5a)-(B.1-5d) illustrate that while the moments up to third order are identical to cumulants for zero mean stationary random processes, the generation of the fourth-order cumulant sequence requires knowledge of the fourth-order moment and autocorrelation sequences.

By putting the delays = 0 in equations (B.1-5a)-(B.1-5d) with the zero mean assumption, the variance, skewness, and kurtosis become

$$\begin{aligned}
\gamma_2^x &= c_2^x(0) = E\{x^2(k)\} \quad (\text{variance}) \\
\gamma_3^x &= c_3^x(0,0) = E\{x^3(k)\} \quad (\text{skewness}) \\
\gamma_4^x &= c_4^x(0,0,0) = E\{x^4(k)\} - 3[\gamma_2^x]^2 \quad (\text{kurtosis})
\end{aligned} \tag{B.1-6}$$

## B.2 HIGHER-ORDER SPECTRA

Higher-order spectra of stochastic signals are usually defined in terms of cumulants and not moments for two reasons: (1) for a stationary Gaussian random process, all of the moments for  $n > 2$ , although generally non-zero, provide no new information, while the fact that the joint cumulants for  $n > 2$  are identically zero conveys this explicitly; (2) if the random variables  $\{x_1, \dots, x_n\}$  can be divided into any two or more groups which are statistically

independent, their  $n$ th-order cumulants are identically zero thus providing a measure of statistical independence. (The  $n$ th-order moments are non-zero.)

Assuming that the cumulant sequence is bounded, i.e., satisfies the condition

$$\sum_{\tau_1=-\infty}^{\infty} \dots \sum_{\tau_{n-1}=-\infty}^{\infty} |c_n^x(\tau_1, \dots, \tau_{n-1})| < \infty, \text{ the } n\text{th-order cumulant spectrum } C_n^x(\omega_1, \dots, \omega_{n-1})$$

of  $\{x(k)\}$  exists and is continuous and is defined as the  $(n-1)$ -dimensional Fourier transform of the  $n$ th-order cumulant sequence

$$\begin{aligned} C_n^x(\omega_1, \omega_2, \dots, \omega_{n-1}) &= \frac{1}{(2\pi)^{n-1}} \sum_{\tau_1=-\infty}^{\infty} \dots \sum_{\tau_{n-1}=-\infty}^{\infty} \\ &\quad \cdot c_n^x(\tau_1, \tau_2, \dots, \tau_{n-1}) \\ &\quad \cdot \exp\{-j(\omega_1 \tau_1 + \omega_2 \tau_2 + \dots + \omega_{n-1} \tau_{n-1})\} \\ &\quad |\omega_i| \leq \pi \text{ for } i = 1, 2, \dots, n-1 \text{ and } |\omega_1 + \omega_2 + \dots + \omega_{n-1}| \leq \pi. \end{aligned} \tag{B.2-1}$$

In general,  $C_n^x(\omega_1, \omega_2, \dots, \omega_{n-1})$  is complex for  $n > 2$ , i.e., it has magnitude and phase.

$$C_n^x(\omega_1, \dots, \omega_{n-1}) = |C_n^x(\omega_1, \dots, \omega_{n-1})| \exp j \psi_n^x(\omega_1, \dots, \omega_{n-1}). \tag{B.2-2}$$

The cumulant spectrum is also periodic with period  $2\pi$ , i.e.,

$$C_n^x(\omega_1, \dots, \omega_{n-1}) = C_n^x(\omega_1 + 2\pi, \dots, \omega_{n-1} + 2\pi).$$

The power spectrum, bispectrum, and trispectrum are special cases of the  $n$ th-order cumulant spectrum defined by equation (B.2-1),

**Power Spectrum:  $n = 2$**

$$C_2^x(\omega) = \frac{1}{2\pi} \sum_{\tau=-\infty}^{\infty} c_2^x(\tau) \exp\{-j(\omega\tau)\} \quad (\text{B.2-3})$$

$$|\omega| \leq \pi,$$

where  $c_2^x(\tau)$  is the covariance sequence of  $\{x(k)\}$  given by equation (B.1-5b). From equation (B.1-5b) and equation (B.2-3) we have

$$c_2^x(\tau) = c_2^x(-\tau)$$

$$C_2^x(\omega) = C_2^x(-\omega) \quad (\text{B.2-4})$$

$$C_2^x(\omega) \geq 0 \quad (\text{real, nonnegative function}).$$

**Bispectrum:  $n = 3$**

$$C_3^x(\omega_1, \omega_2) = \frac{1}{(2\pi)^2} \sum_{\tau_1=-\infty}^{\infty} \sum_{\tau_2=-\infty}^{\infty} c_3^x(\tau_1, \tau_2) \exp\{-j(\omega_1\tau_1 + \omega_2\tau_2)\}$$

$$|\omega_1| \leq \pi, |\omega_2| \leq \pi, |\omega_1 + \omega_2| \leq \pi,$$

(B.2-5)

where  $c_3^x(\tau_1, \tau_2)$  is the third-order cumulant sequence of  $\{x(k)\}$  described by equation (B.1-

5c). Important symmetry conditions follow from equation (B.1-5c)

$$\begin{aligned}
c_3^x(\tau_1, \tau_2) &= c_3^x(\tau_2, \tau_1) = c_3^x(-\tau_2, \tau_1 - \tau_2) \\
&= c_3^x(\tau_2 - \tau_1, -\tau_1) = c_3^x(\tau_1 - \tau_2, -\tau_2) \quad (\text{B.2-6}) \\
&= c_3^x(-\tau_1, \tau_2 - \tau_1).
\end{aligned}$$

The definition of the bispectrum in equation (B.2-5) and the properties of third-order cumulants in equation (B.2-6) give

$$\begin{aligned}
C_3^x(\omega_1, \omega_2) &= C_3^x(\omega_2, \omega_1) = C_3^{x*}(-\omega_2, -\omega_1) \\
&= C_3^{x*}(-\omega_1, -\omega_2) = C_3^x(-\omega_1 - \omega_2, \omega_2) \quad (\text{B.2-7}) \\
&= C_3^x(\omega_1, -\omega_1 - \omega_2) = C_3^x(-\omega_1 - \omega_2, \omega_1) \\
&= C_3^x(\omega_2, -\omega_1 - \omega_2).
\end{aligned}$$

This knowledge of the bispectrum in the triangular region  $\omega_2 \geq 0$ ,  $\omega_1 \geq \omega_2$ ,  $\omega_1 + \omega_2 \leq \pi$  is enough for a complete description of the bispectrum.

*Trispectrum:  $n = 4$*

$$\begin{aligned}
C_4^x(\omega_1, \omega_2, \omega_3) &= \frac{1}{(2\pi)^3} \sum_{\tau_1=-\infty}^{\infty} \sum_{\tau_2=-\infty}^{\infty} \sum_{\tau_3=-\infty}^{\infty} c_4^x(\tau_1, \tau_2, \tau_3) \\
&\quad \cdot \exp\{-j(\omega_1 \tau_1 + \omega_2 \tau_2 + \omega_3 \tau_3)\} \quad (\text{B.2-8}) \\
|\omega_1| &\leq \pi, |\omega_2| \leq \pi, |\omega_3| \leq \pi, |\omega_1 + \omega_2 + \omega_3| \leq \pi,
\end{aligned}$$

where  $c_4^x(\tau_1, \tau_2, \tau_3)$  is the fourth-order cumulant sequence given by equation (B.1-5d).

Symmetry properties can be derived for the trispectrum, similar to those given in equation (B.2-7) for the bispectrum.

A normalized cumulant spectrum which combines the cumulant spectrum of order  $n$ ,  $C_n^x(\omega_1, \dots, \omega_{n-1})$ , and the power spectrum,  $C_2^x(\omega)$ , of a process may be defined as

$$P_n^x(\omega_1, \omega_2, \dots, \omega_{n-1}) \triangleq \frac{C_n^x(\omega_1, \omega_2, \dots, \omega_{n-1})}{[C_2^x(\omega_1) \cdot C_2^x(\omega_2) \cdots C_2^x(\omega_{n-1}) \cdot C_2^x(\omega_1 + \omega_2 + \dots + \omega_{n-1})]^{1/2}} \quad (\text{B.2-9})$$

The third-order ( $n = 3$ ) case is called the bicoherence which is the normalized bispectrum

$$P_3^x(\omega_1, \omega_2) \triangleq \frac{C_3^x(\omega_1, \omega_2)}{[C_2^x(\omega_1) C_2^x(\omega_2) C_2^x(\omega_1 + \omega_2)]^{1/2}} \quad (\text{B.2-10})$$

where  $C_3^x$  is defined in equation (B.2-5) and  $C_2^x$  is defined in equation (B.2-3).

The six symmetry regions of the third-order cumulant as given in equation (B.2-6) and the twelve symmetry regions of the bispectrum as given in equation (B.2-7) are listed below and shown in Figures B.2-1a and B.2-1b:

## cumulant symmetries

1.  $c_3^x(\tau_1, \tau_2)$
2.  $c_3^x(\tau_2, \tau_1)$
3.  $c_3^x(-\tau_2, \tau_1 - \tau_2)$
4.  $c_3^x(-\tau_1, \tau_2 - \tau_1)$
5.  $c_3^x(\tau_2 - \tau_1, -\tau_1)$
6.  $c_3^x(\tau_1 - \tau_2, -\tau_2)$

## bispectrum symmetries

1.  $C_3^x(\omega_1, \omega_2)$
2.  $C_3^x(\omega_2, \omega_1)$
3.  $C_3^{x*}(-\omega_2, \omega_1 + \omega_2)$
4.  $C_3^{x*}(-\omega_1, \omega_1 + \omega_2)$
5.  $C_3^x(-\omega_1 - \omega_2, \omega_1)$
6.  $C_3^x(-\omega_1 - \omega_2, \omega_2)$
7.  $C_3^{x*}(\omega_1, -\omega_2)$
8.  $C_3^{x*}(-\omega_2, -\omega_1)$
9.  $C_3^x(\omega_2, -\omega_1 - \omega_2)$
10.  $C_3^x(\omega_1, -\omega_1 - \omega_2)$
11.  $C_3^{x*}(\omega_1 + \omega_2, -\omega_1)$
12.  $C_3^{x*}(\omega_1 + \omega_2, -\omega_2)$

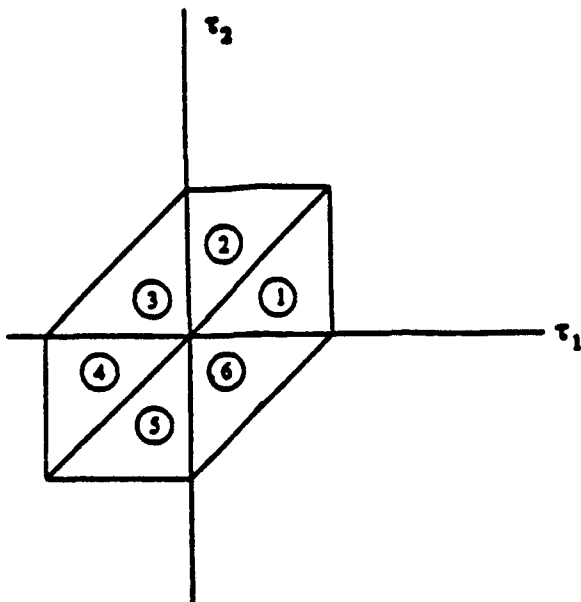


**Figure B.2-1a**

The six symmetry regions of the third order cumulant function  $C_3^x(\tau_1, \tau_2)$

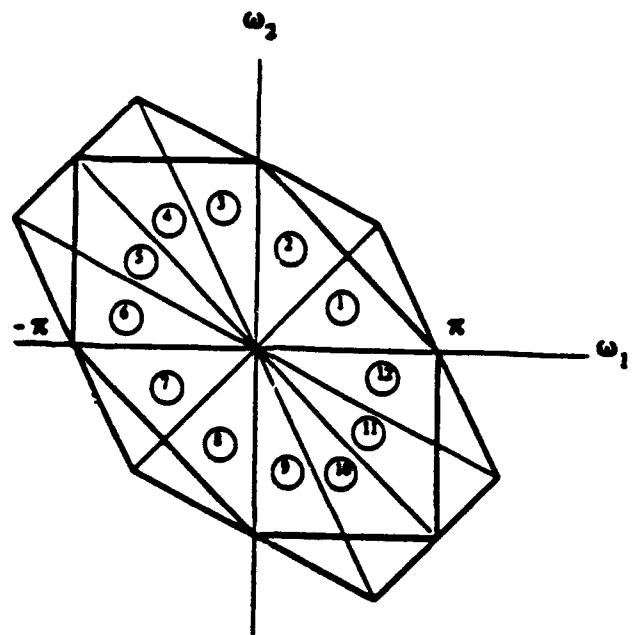


**Figure B.2-1b**

The twelve symmetry regions of the bispectrum  $C_3^x(\omega_1, \omega_2)$

The additional symmetries as defined by the extremities of the outer hexagon in the above figure are due to the effects of a discrete time/continuous frequency bispectrum as opposed to the standard inner hexagon symmetry region of the continuous time bispectrum corresponding to a band limited process. The net result is an additional set of twelve symmetry regions defining the borders of the outer hexagon. The double periodicity of the bispectrum causes this effect and is illustrated in a Figure B.2-2 from Allison.<sup>24</sup> The block capital "C" notation defines conjugate symmetry regions of the bispectrum while the boxed numbers donate equivalent regions of the discrete time bispectrum. Figure B.2-2 reflects a normalized sampling frequency = 1 with the lighter shaded region being the zero part of the bispectrum for a bandlimited process indicative of a properly sampled, stationary time series. The darker shaded region represents the non-zero part of the bispectrum.

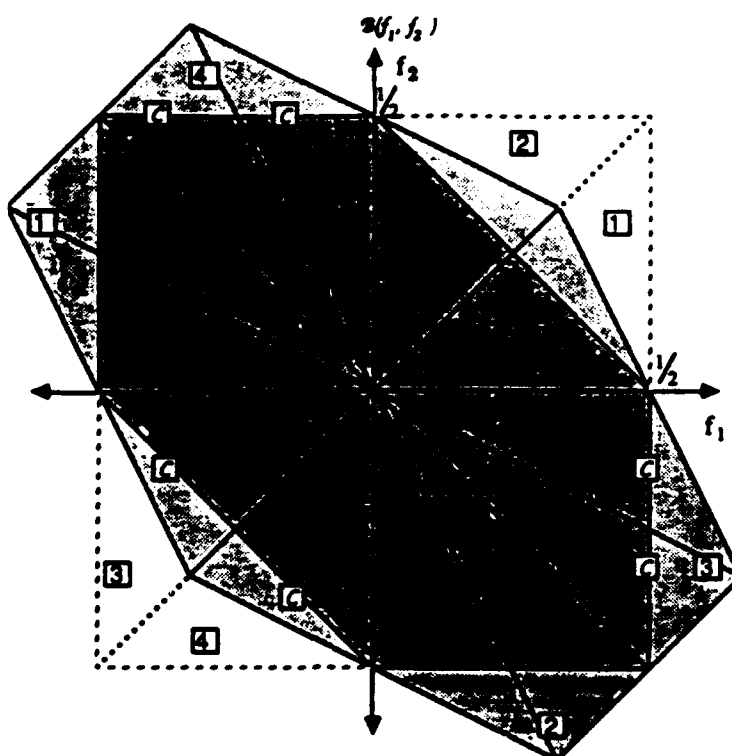
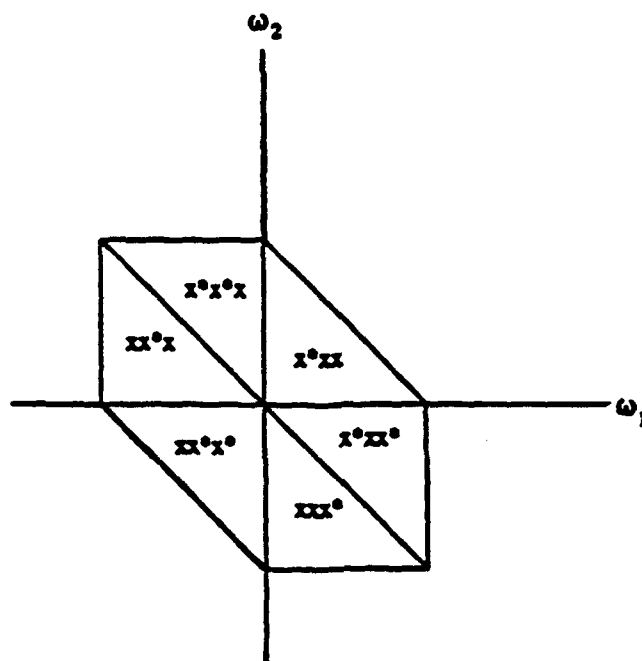


Figure B.2-2 Fundamental Domain of Discrete Time Bispectrum

Previous bispectrum properties apply solely to real-valued signals. The extension to complex-valued signals has not been widely addressed. The following definitions and properties are due to the requirement for complex signals for radar signal processing as presented in Jouny.<sup>23</sup> This is a normal requirement for analytic signal analysis for a wide spectrum of applications involving real or quadrature-sampled data.

If the data  $\{x(k)\}$  is a complex stationary process, the second order cumulant is defined as  $c_2^x(\tau) = E\{x^*(k)x(k+\tau)\}$ . It is also possible to alternate the conjugate so that  $c_2^x(\tau) = E\{x(k)x^*(k+\tau)\}$ . For the third joint cumulant case, the conjugate can be placed either on one or two entries of the triple product in equation (B.1-5c). Only one placement,

however, defines which one of the symmetry relations given in equation (B.2-7) remains valid. In general, the bispectrum of complex signals has twofold symmetry about an axis defined on  $\{\omega_1 = \omega_2, \omega_2 = -.5\omega_1, \omega_1 = -.5\omega_2, \omega_1 = -\omega_2\}$ . See Figure B.2-3 for the distributions of responses in the bispectral domain as a function of the placement of the conjugates for the third order cumulants.



**Figure B.2-3** Distribution of the responses in the bispectral domain as a function of third order cumulant conjugate placement

For example, if the first quadrant  $\omega_1, \omega_2 > 0$  is preferred then the third order cumulant is

defined as  $c_3^x(\tau_1, \tau_2) = E\{x^*(k)x(k+\tau_1)x(k+\tau_2)\}$ .

The following relations define the bispectrum of complex-valued signals for all possible positions of the complex conjugate:

$$E\{x^*(k)x(k+\tau_1)x(k+\tau_2)\} \xrightarrow{F} \langle X(\omega_1)X(\omega_2)X^*(\omega_1+\omega_2) \rangle$$

with the symmetry relation  $C_3^x(\omega_1, \omega_2) = C_3^x(\omega_2, \omega_1)$ ,

$$E\{x(k)x^*(k+\tau_1)x(k+\tau_2)\} \xrightarrow{F} \langle X^*(-\omega_1)X(\omega_2)X(-\omega_1-\omega_2) \rangle$$

with the symmetry relation  $C_3^x(\omega_1, \omega_2) = C_3^x(\omega_1, -\omega_1-\omega_2)$ ,

$$E\{x(k)x(k+\tau_1)x^*(k+\tau_2)\} \xrightarrow{F} \langle X(\omega_1)X^*(-\omega_2)X(-\omega_1-\omega_2) \rangle$$

with the symmetry relation  $C_3^x(\omega_1, \omega_2) = C_3^x(-\omega_1-\omega_2, \omega_2)$ ,

$$E\{x(k)x^*(k+\tau_1)x^*(k+\tau_2)\} \xrightarrow{F} \langle X^*(-\omega_1)X^*(-\omega_2)X(-\omega_1-\omega_2) \rangle$$

with the symmetry relation  $C_3^x(\omega_1, \omega_2) = C_3^x(\omega_2, \omega_1)$ ,

$$E\{x^*(k)x^*(k+\tau_1)x(k+\tau_2)\} \xrightarrow{F} \langle X^*(-\omega_1)X(\omega_2)X^*(\omega_1+\omega_2) \rangle$$

with the symmetry relation  $C_3^x(\omega_1, \omega_2) = C_3^x(-\omega_2-\omega_1, \omega_2)$ ,

$$E\{x^*(k)x(k+\tau_1)x^*(k+\tau_2)\} \xrightarrow{F} \langle X(\omega_1)X^*(-\omega_2)X^*(\omega_1+\omega_2) \rangle$$

with the symmetry relation  $C_3^x(\omega_1, \omega_2) = C_3^x(\omega_1, -\omega_1-\omega_2)$ ,

where  $\xrightarrow{F}$  denotes the Fourier transform pair and  $\langle \rangle$  denotes the ensemble average.

The triple correlation aspect of the bispectrum is self evident from its definition as the Fourier transform of a third order cumulant in equation (B.2-1). This definition implies that the bispectrum at a particular frequency pair  $(\omega_p, \omega_q)$  is non-zero if at least one of the three spectral responses  $X(\omega_p)$ ,  $X(\omega_q)$ , and  $X(\omega_p + \omega_q)$  is correlated with the other two since

$$C_3^2(\omega_p, \omega_q) = \langle X(\omega_p)X(\omega_q)X^*(\omega_p + \omega_q) \rangle.$$

This definition arises from a Fourier-Stieltjes representation of  $X$  where the distinction is made between the power spectrum representation of the contribution to the mean product of two Fourier components whose frequencies are the same compared to the similar bispectrum contribution involving three Fourier components where one frequency equals the sum of the other two.<sup>15</sup>

**APPENDIX C.**

**SIMULATED/REAL DATA TEST RESULTS**

## **C.0 POWER SPECTRUM/BISPECTRUM COMPARISON FOR SIMULATED DATA**

Figures C.0-1 through C.0-3 show a comparison between the power spectrum and bispectrum of a harmonic (pure tone) for three different states: (1) noiseless (Figure C.0-1), (2) low noise (Figure C.0-2), and (3) high noise (Figure C.0-3). The low and high noise states represent signal-to-noise ratios (SNR) of 16.5 and -3.5 dB respectively where the SNR is defined as the ratio of the signal variance to the noise variance; when expressed in dB, it is given by  $10 \log (\sigma_s^2 / \sigma_n^2)$  where  $\sigma_s^2$  is the variance of the signal and  $\sigma_n^2$  is the variance of the noise. The bispectrum was computed using a FFT size of 256 corresponding to the data length as no averaging was performed. The bispectrum slices reflect the effects of no windowing and a Rao Gabr window of length 5 for smoothing purposes. The slices with the highest bispectral value in the triangular region of support were chosen, a convention followed in bispectral processing.<sup>25</sup> The pure tone was designed to show up at .5 hz for this set of test cases with a sampling rate of 2 hz. The noise states were generated by adding Gaussian noise to the pure tone. The plots indicate essentially no difference in the signal peak to noise level representations between the power spectrum and bispectrum for the noise states in Figures C.0-2 and C.0-3 respectively.

## **C.1 DIRECT/INDIRECT BISPECTRUM COMPARISON FOR SIMULATED DATA**

Figures C.1-1 and C.1-2 show a comparison between the conventional direct and indirect methods for estimating the bispectrum as defined in sections 2.1.1 and 2.1.2 respectively. The data for the figures was generated using the Hi-Spec program "qpc\_gen" which generates quadratically phase-coupled harmonics in noise as defined in section A.0 of Appendix A. Figure C.1-1 represents bispectral processing using a quadratically phase coupled

synthetic consisting of three quadratically phase coupled harmonics at frequencies  $f_1 = 0.12$ ,  $f_2 = 0.18$ , and  $f_3 = f_1 + f_2 = 0.30$  Hz. The data was segmented to reflect independent realizations. For each realization the phases of the first two harmonics were chosen randomly with the phase of the third harmonic set to the sum of the phases of the first two. A total of 64 independent realizations, each consisting of 64 samples, were generated. The amplitudes of all three harmonics were unity and the signal was noise free. Figure C.1-2 data was identical to Figure C.1-1 with the exception that Gaussian noise was added to the signal to obtain an overall signal-to-noise ratio of 0 dB.

The direct bispectrums from left to right reflect no windowing and a Rao-Gabr window of length 5 respectively. Similarly, the indirect bispectrums from left to right reflect no windowing and a Parzen window respectively. The FFT size in both cases was 128 with the number of lags chosen in the indirect case for the estimation of the higher order moments being 21. (It is suggested as a rule of thumb in Hi-Spec that the number of lags should be set to the number of samples per segment divided by 10.)

The severe deterioration of the indirect bispectrum estimate for the noisy data in Figure C.1-2 was unexpected relative to the successful suppression of noise noted for the direct bispectrum estimate in comparison. The skewness of the noiseless data in Figure C.1-1, a function of the quadratic phase coupling, was 0.82 indicating highly skewed data. The skewness of the noisy data in Figure C.1-2 was 0.36 indicative that the phase coupling contribution to the skewness was not masked by the addition of Gaussian noise. It is worthwhile to note that for the generation of uncoupled sinusoids at the same frequencies, 0.12, 0.18, and 0.30 Hz, the noiseless skewness was 0.03 while the noisy skewness was -0.01 indicative of symmetry which explains the inability of the bispectrum to differentiate uncoupled sinusoids from symmetric pdf noise.

The indirect bispectrum's inability to sufficiently suppress the noise in Figure C.1-2 along with resolution problems noted in Figure C.1-1 (note the loss of the quadratic phase coupled triplet in the Parzen window case) dictated the use of the direct bispectrum for comparison against second order statistical methods for this paper. The problems related to the indirect bispectrum remain unresolved at this time pending further study in regard to the theory and algorithmic implementation in Hi-Spec.

## **C.2 POWER SPECTRUM/BISPECTRUM COMPARISON FOR REAL DATA**

Figures C.2-1 and C.2-2 show a comparison between the power spectrum and direct bispectrum as defined in equations (B.2-3) through (B.2-7) respectively of Appendix B. The bispectrum was computed using a FFT size = 128 with a Rao-Gabr window of length 3. Figure C.2-1 is a sonar ping using a 100 ms hop code designated Ping A while Figure C.2-2 is a 11 ms pure tone designated Ping B. The 1-quadrant bispectrum is shown via contour plots with the quadrant symmetry clearly evident as illustrated by the figures in section B.2, in particular Figure B.2-3, "Distribution of the responses in the bispectral domain as a function of third order cumulant conjugate placement," which is in the first quadrant for Hi-Spec. Bispectrum slices are computed following the convention referenced in section C.0 for comparison with the power spectrum. The ping data limitations constrain the averaging to approximately 9 segments which mirrors the tests performed in Wilson.<sup>29</sup> The frequency scales have been normalized for sanitization purposes and the power spectrum/bispectrum comparison reflects a relative dB scale as a log power spectrum/log magnitude bispectrum is computed - a parameter typically found in the literature.

The figures indicate that no processing gain is realized by the bispectrum over the power spectrum for detection purposes in both instances. Closer examination of the statistics

reveals that the distributions of the returns had skewness measures of (-0.02, 0.00) and (0.02, 0.01) respectively for their real/imaginary parts. Moreover, the kurtosis statistics were (3.68, 3.15) and (3.19, 3.21) respectively (a kurtosis of 3 indicates Gaussianity). Clearly, the desired effects of target dynamics and/or modulation necessary to skew the data sufficiently for bispectral enhancement via suppression of Gaussian or non-Gaussian symmetric pdf noise were not enough<sup>38-48,49</sup>.

The data analyzed represented shallow water scenarios. A total of approximately 11 pings were examined with the results in all cases similar to those described in Figures C.2-1 and C.2-2. The average echo skewness measure over 11 pings was (0.01, -0.00) with a skewness range of ([-0.03 0.03], [-0.03 0.01]) and a standard deviation of (0.02, 0.01). The average echo kurtosis measure was (3.47, 3.47) with a kurtosis range of ([2.67 4.84], [2.60 4.35]) and a standard deviation of (0.73, 0.54). These numbers appear to be well within the bounds of Gaussianity for skewness with only a slight variance for kurtosis. The corresponding numbers for the reverberation data in the neighborhood of the echoes was (0.00, 0.00) for skewness with range ([-0.01 0.01], [-0.00 0.01]) and standard deviation (0.01, 0.00) which is the crux of the problem, i.e., the echoes cannot be discriminated sufficiently in a statistical sense from the reverberation for successful bispectral processing.

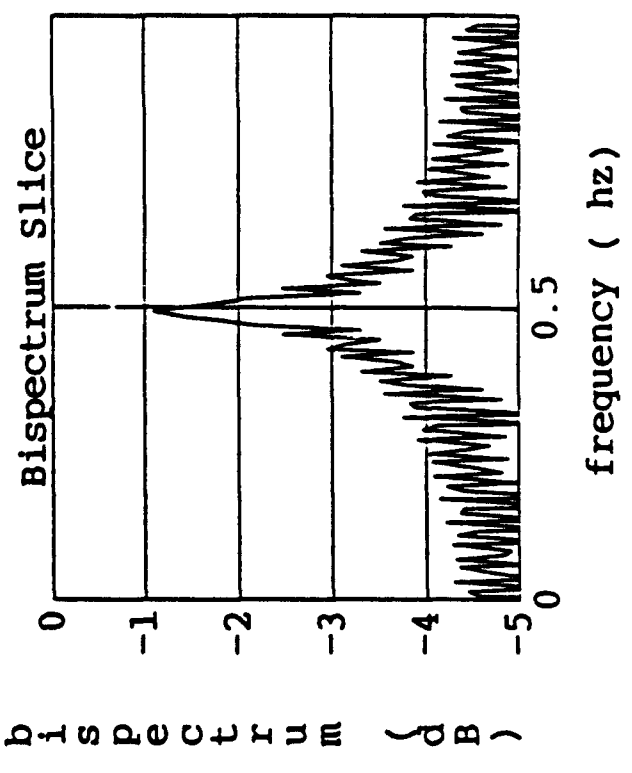
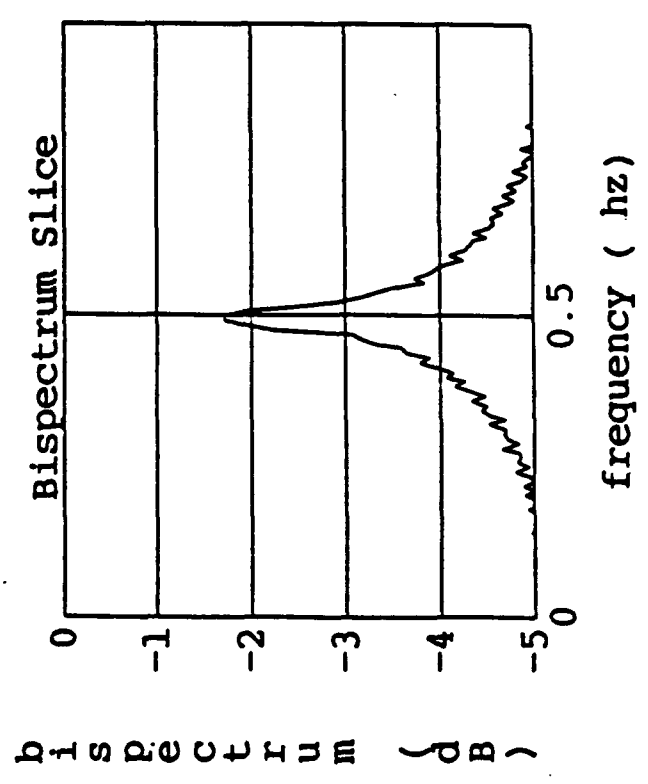
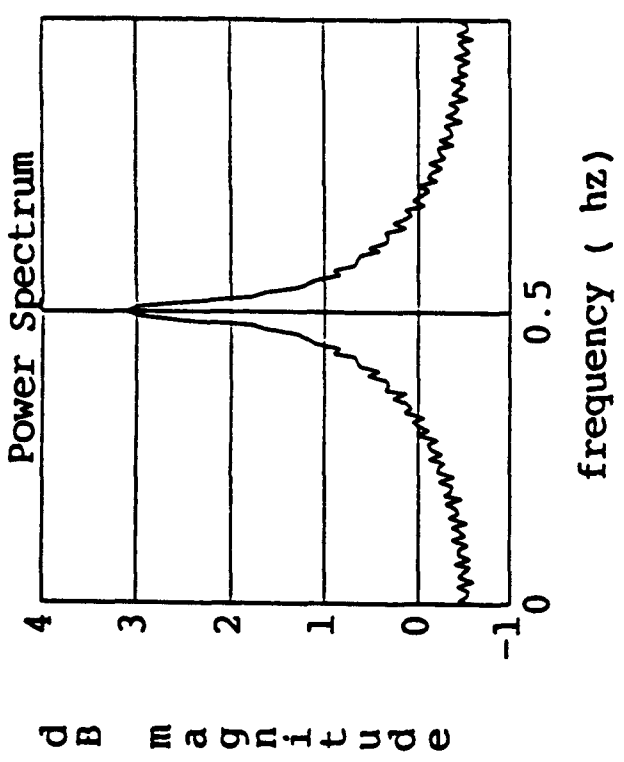
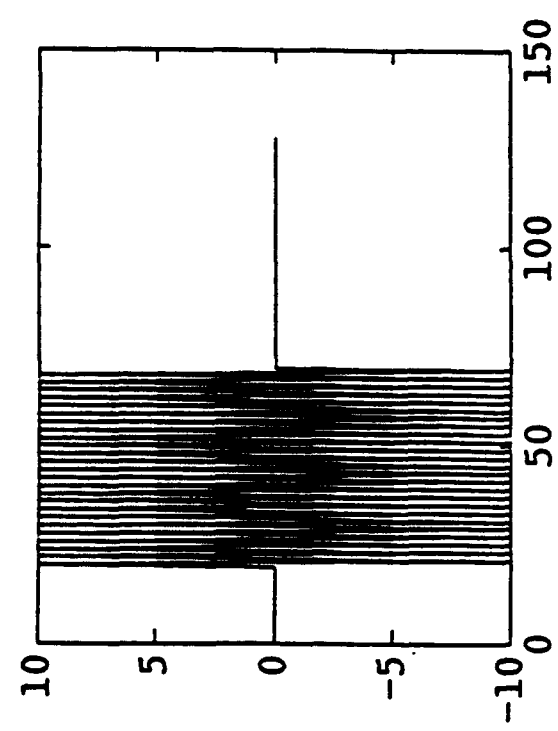


Figure C.0-1 Power Spectrum/Bispectrum Comparison for Simulated Data - Noiseless

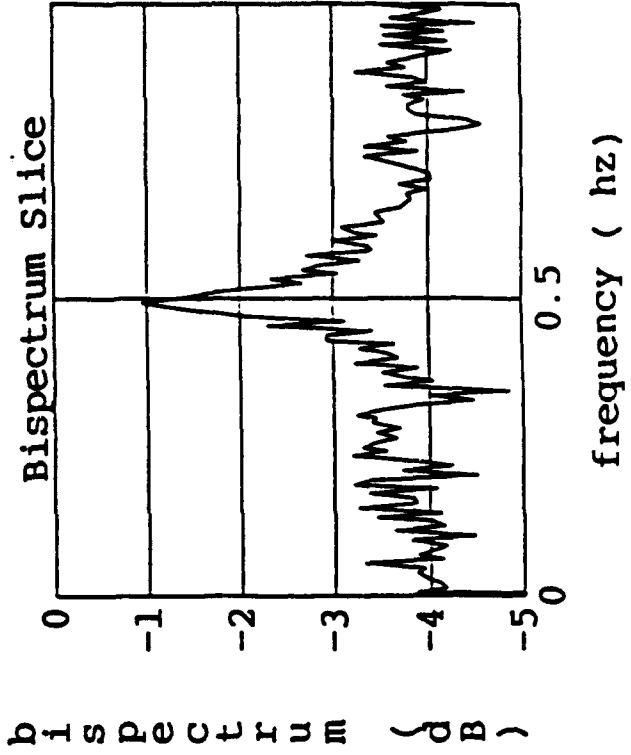
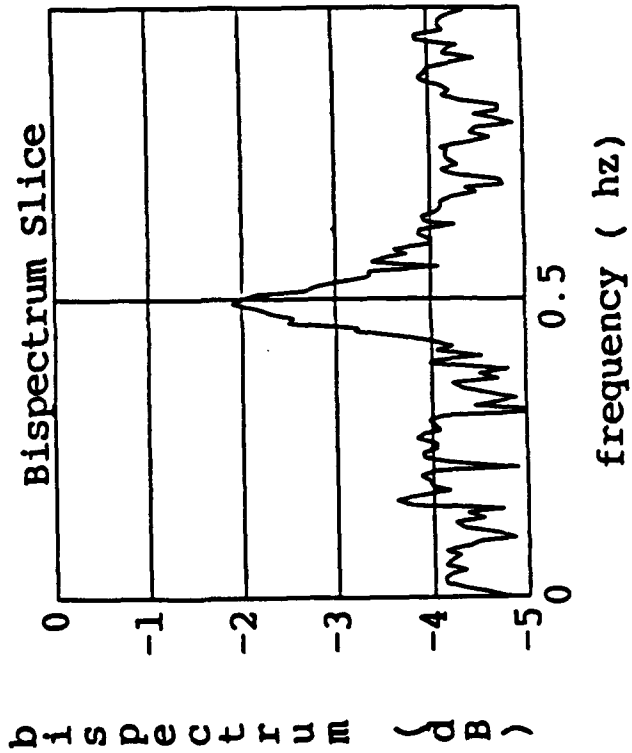
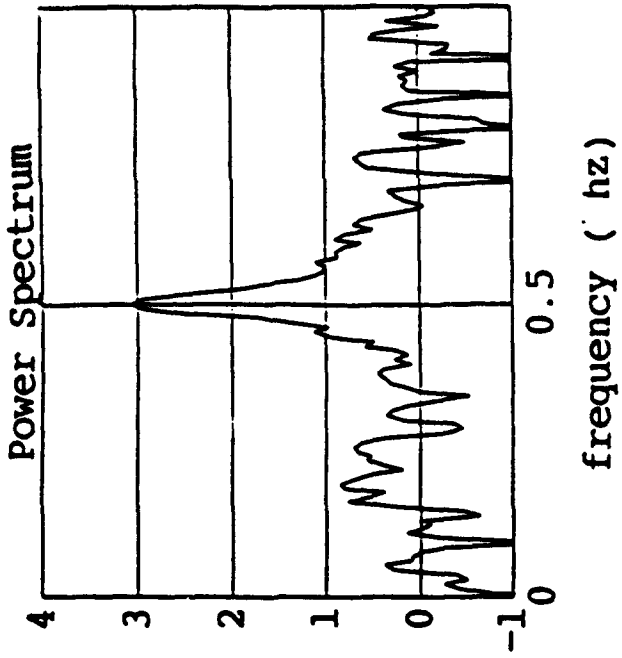
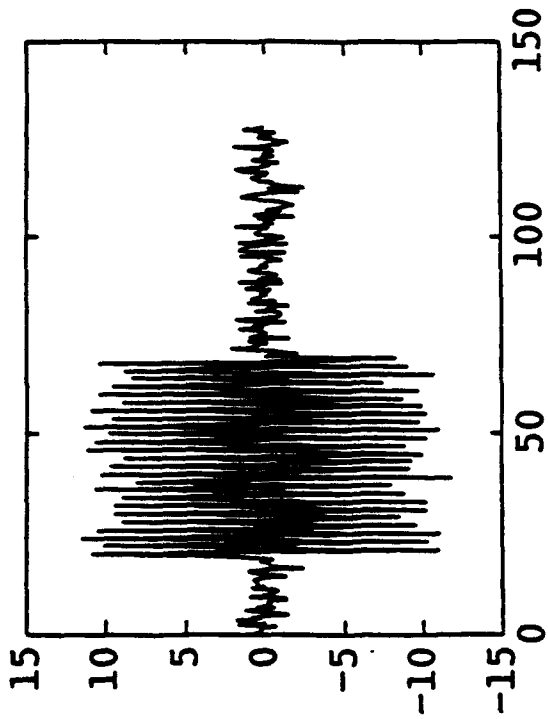


Figure C.0-2 Power Spectrum/Bispectrum Comparison for Simulated Data - Low Noise

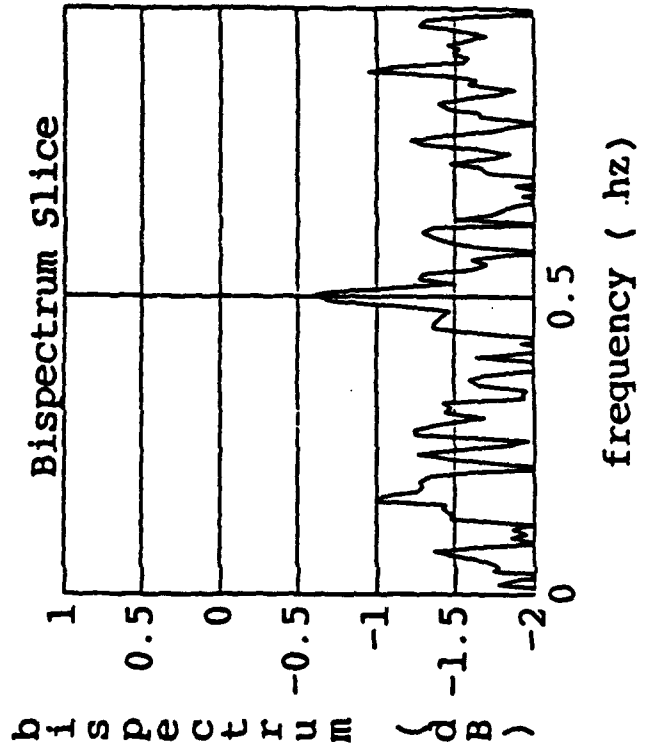
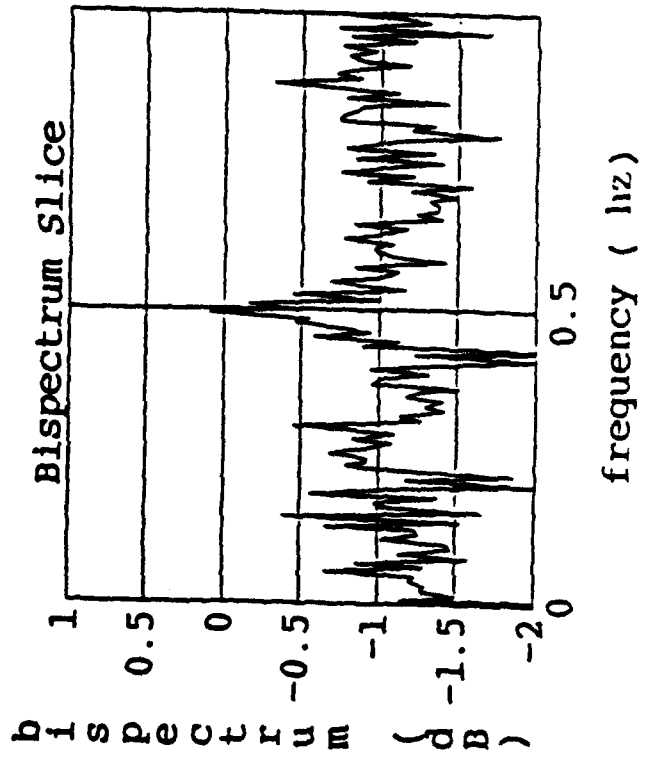
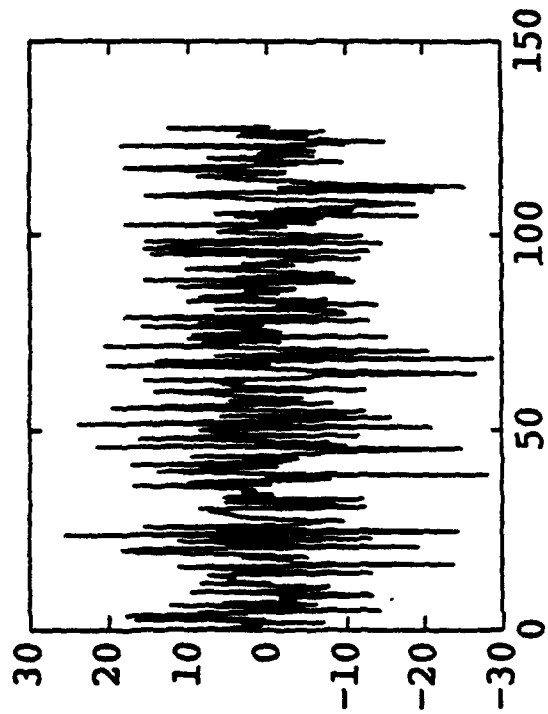
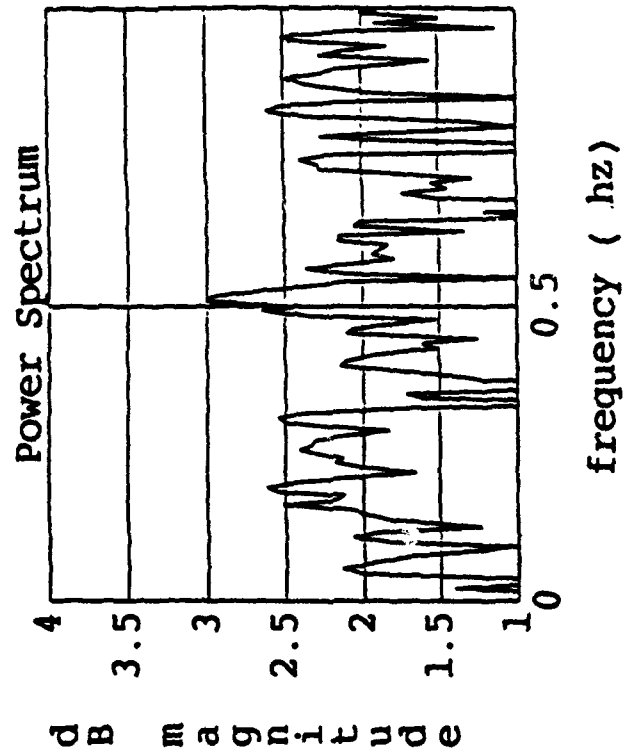


Figure C.0-3 Power Spectrum/Bispectrum Comparison for Simulated Data - High Noise

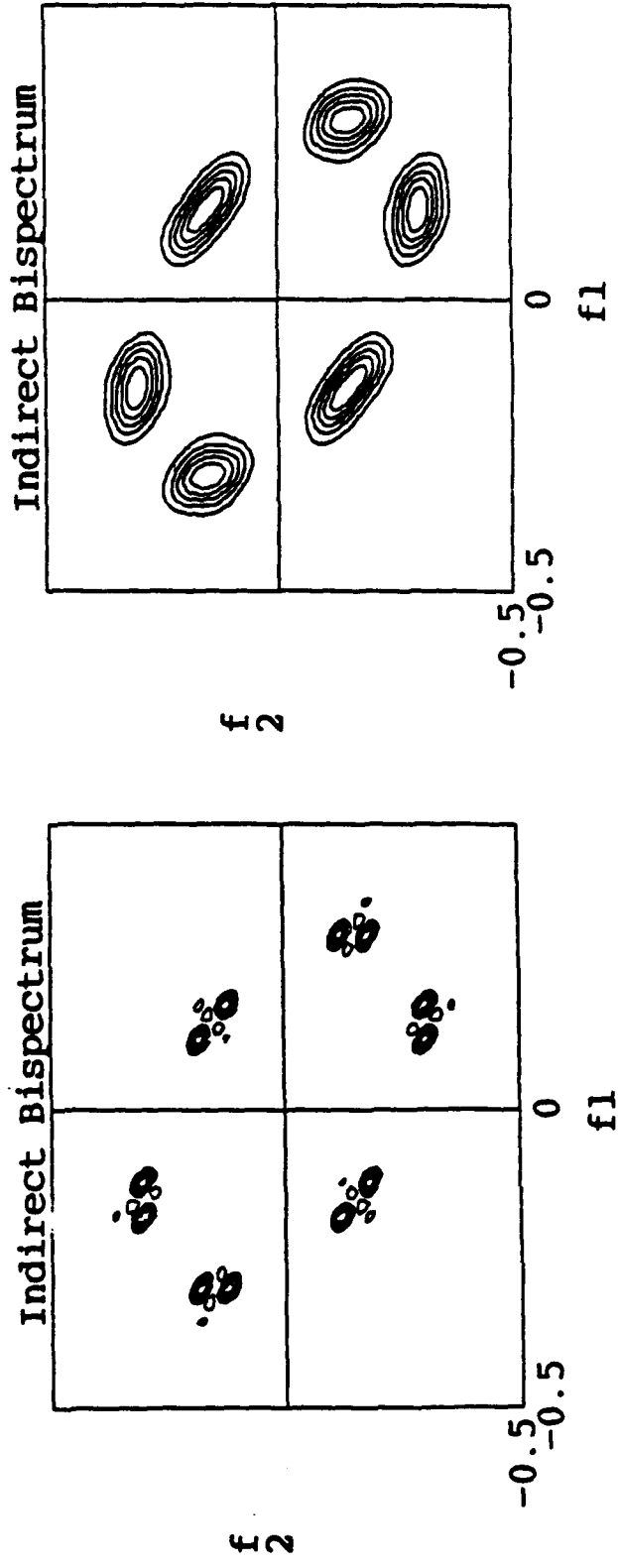
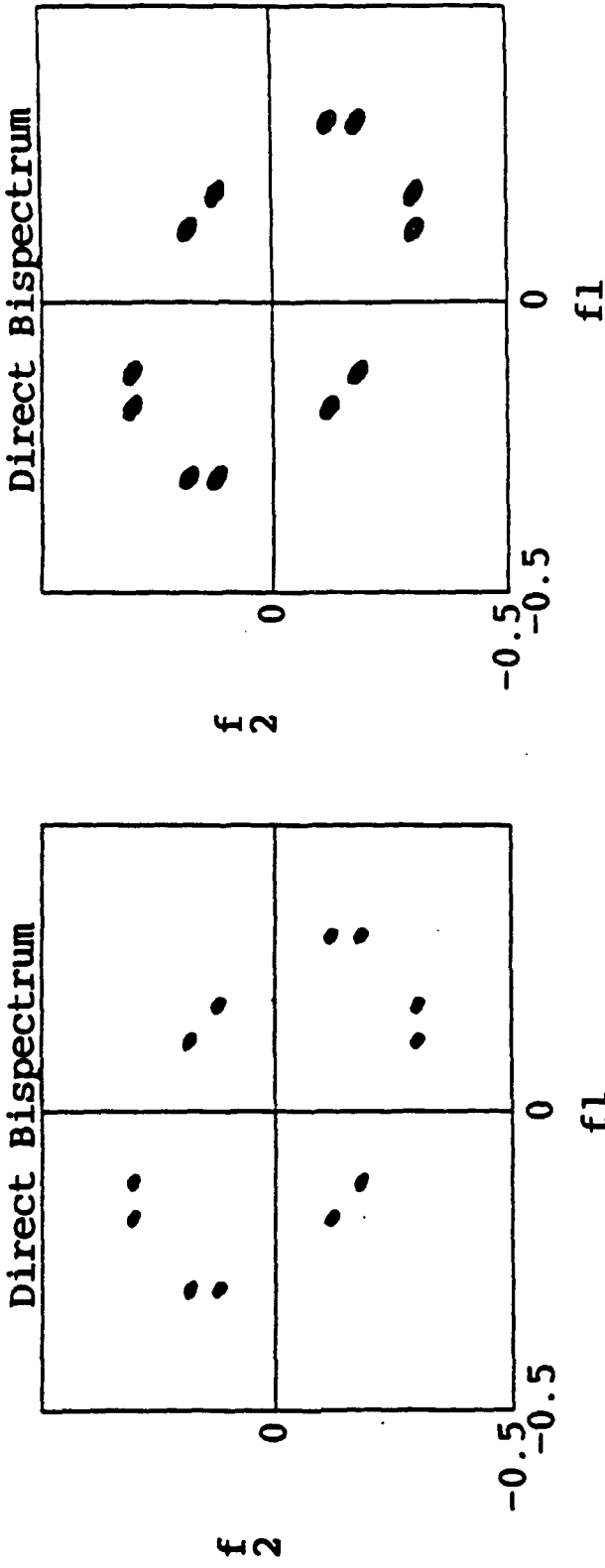


Figure C.1-1 Direct/Indirect Bispectrum Comparison for Simulated Data - Noiseless

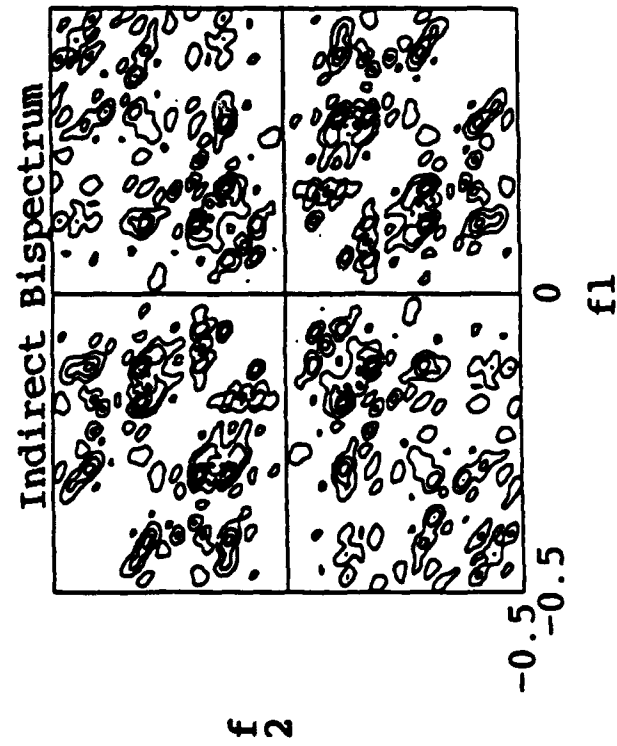
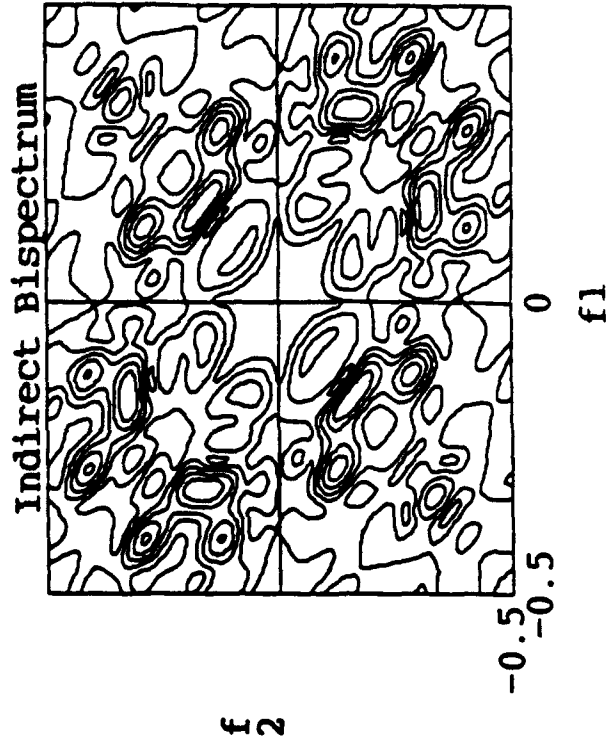
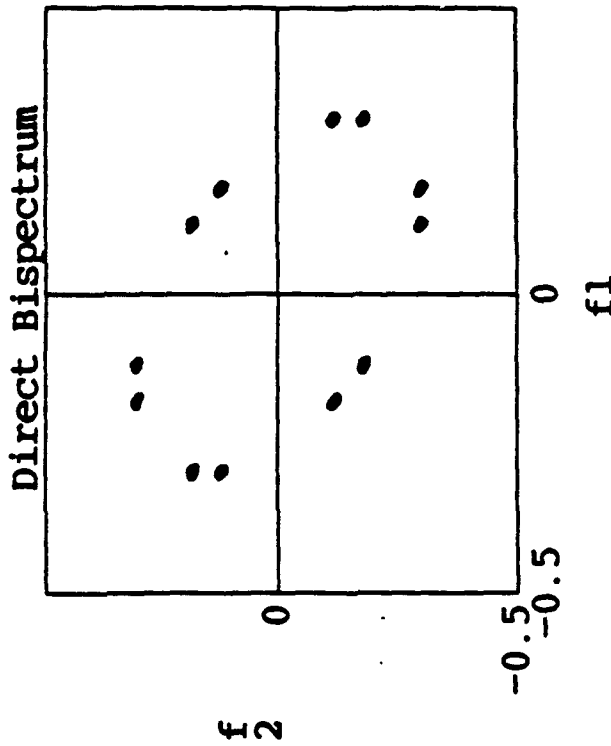
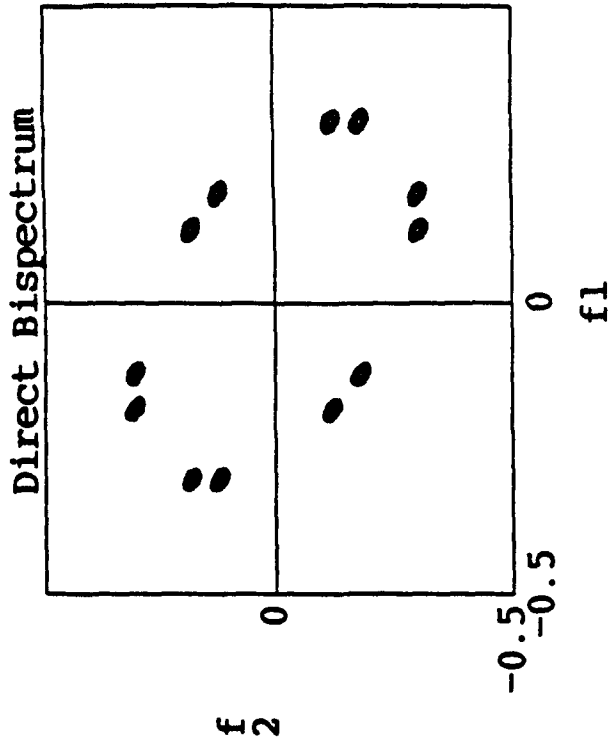


Figure C.1-2 Direct/Indirect Bispectrum Comparison for Simulated Data - Noise

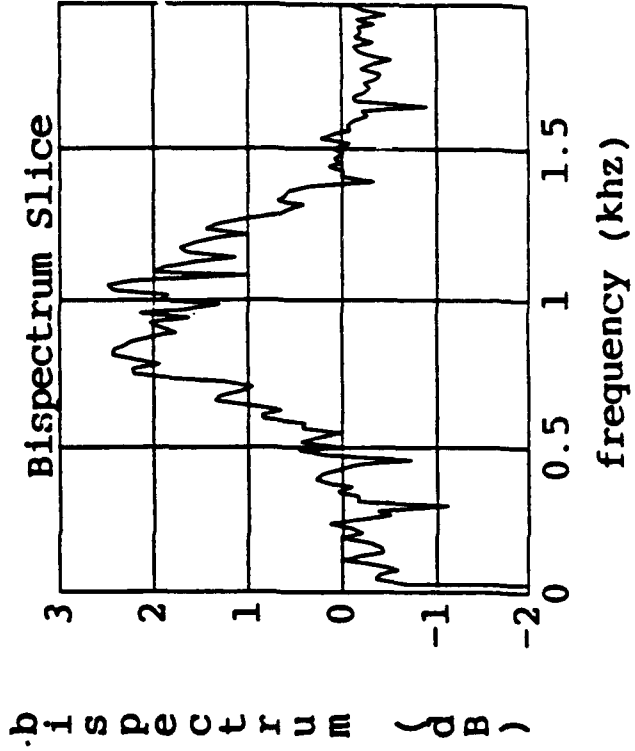
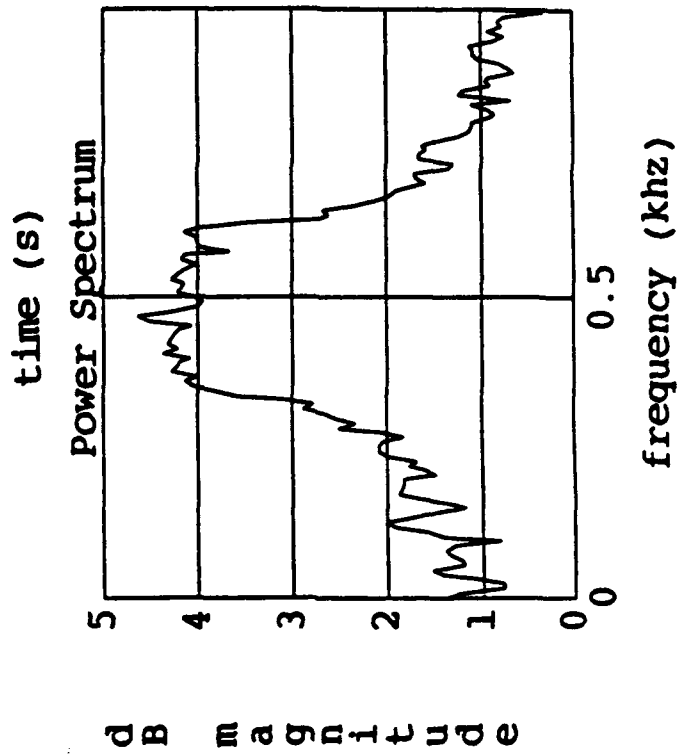
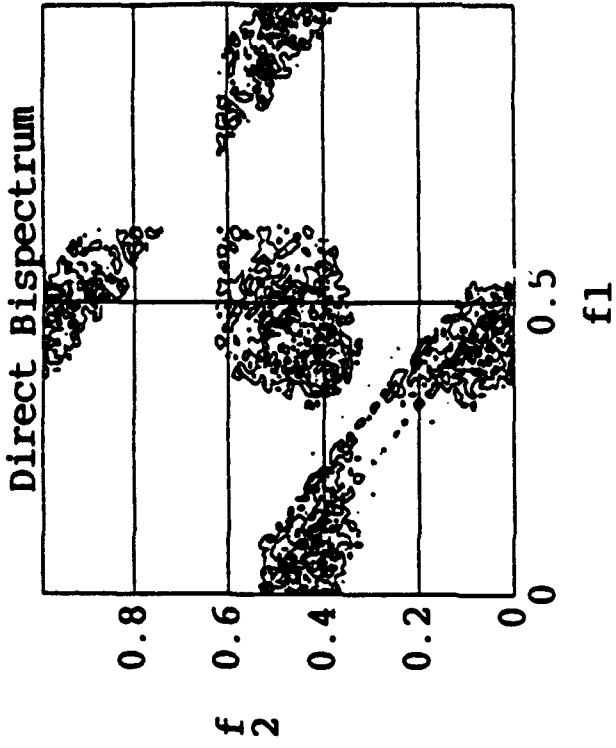
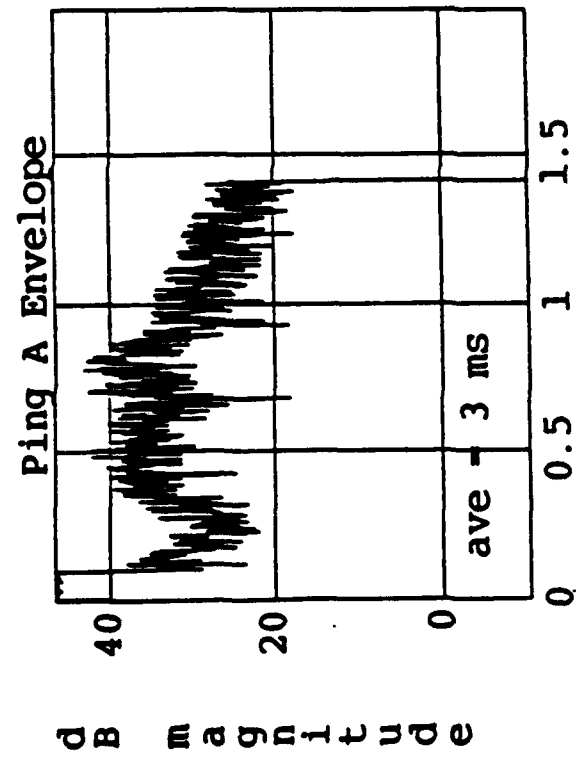


Figure C.2-1 Power Spectrum/Bispectrum Comparison for Real Data - Hop Code

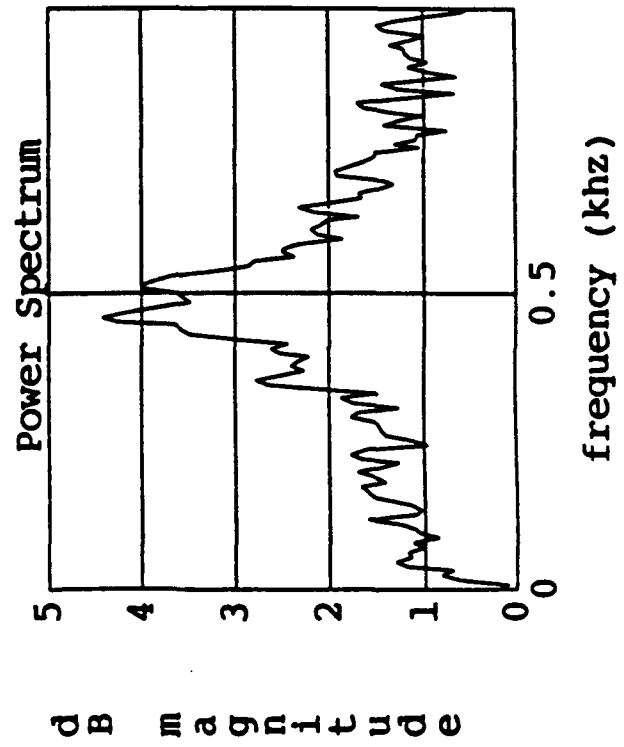
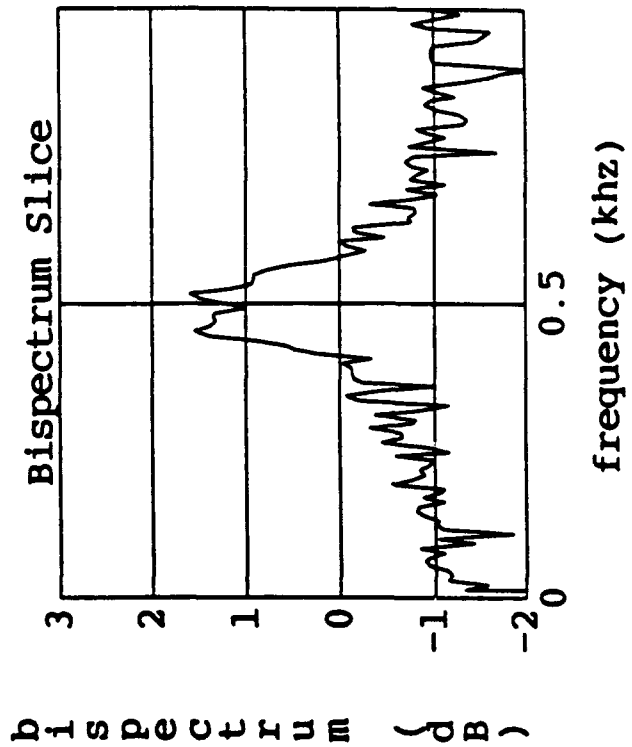
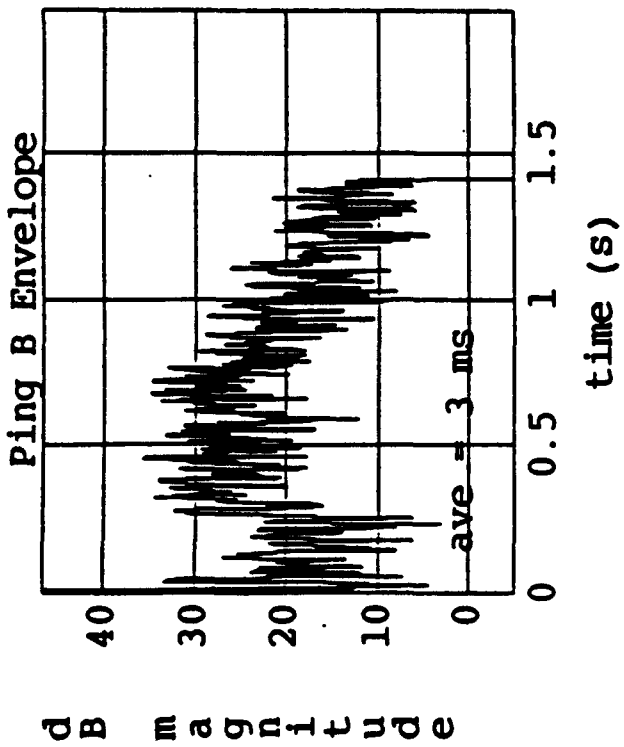
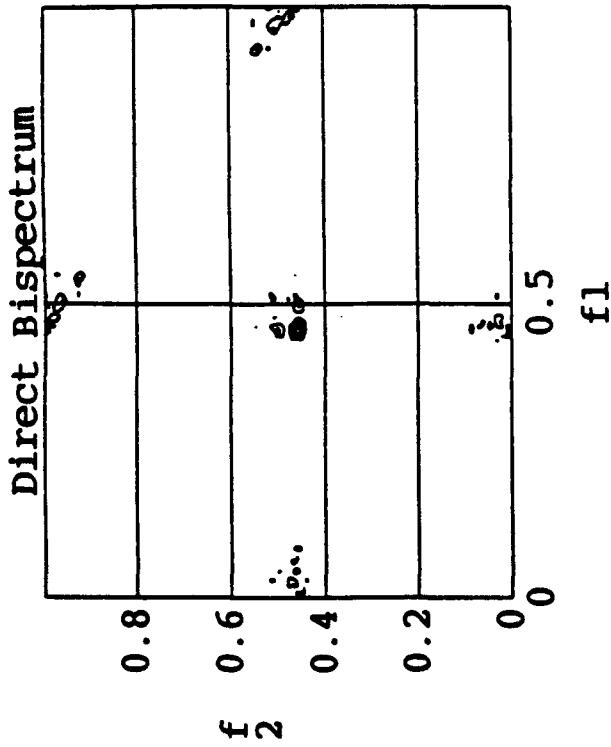


Figure C.2-2 Power Spectrum/Bispectrum Comparison for Real Data - Pure Tone